Karlsruhe Institute of Technology (KIT)
Department of Chemical and Process Engineering
Institute of Mechanical Process Engineering and Mechanics

Master Thesis

Simulation of adsorption on moving particles using the Eulerian-Eulerian lattice Boltzmann method

Florian Raichle

November 08, 2021 - May 23, 2022

Supervisor: Prof. Dr.-Ing. Hermann Nirschl
Advisors: Dr. Mathias Krause, M.Sc. Fedor Bukreev

Abstract

To simulate adsorption in industrial applications and gain more insight into the coupling of fluid flow and adsorption performance, adsorption models at larger scales than just single particles are needed. In this thesis a model of the adsorption on moving particles is applied to the lattice Boltzmann method using an Euler-Euler approach. The adsorption model is based on mass transfer as described by the linear driving force model and can incorporate several mass transfer mechanisms, such as film diffusion, surface diffusion and pore diffusion. Particles, their adsorbate loading, and the solute are described by the advection diffusion equation with an adsorption source term.

Using analytical solutions for a batch and fixed bed reactor the model and its coupling with the fluid is validated. Grid studies are conducted to show the convergence of the model. The applicability of the model to complex flow problems is demonstrated in a static mixer with moving particles.

Lattice Boltzmann Research Group (LBRG)
Institut für Mechanische Verfahrenstechnik und Mechanik (MVM)

Master Thesis

Simulation von Adsorption an bewegten Partikeln mittels eines Euler-Euler Lattice-Boltzmann-Modells
Simulation of adsorption on moving particles using the Eulerian-Eulerian Lattice-Boltzmann method

Student: Florian Raichle
Supervisor: Fedor Bukreev
Timeframe: 08.11.2021 - 09.05.2022

Description

Adsorption plays an important role in many industrial processes and is of great interest especially because of the role it plays in catalysis. It is used in both gas and liquid mixtures, as in water treatment for example to remove contaminants like phosphates. There are many models available that describe adsorption equilibria and kinetics and this field is still the object of active research. A majority of the literature about its application however deals with packed bed reactors, investigations into reactions on moving particles, like they are found in water treatment, are less common.

For the development of processes at an industrial scale it is often impossible to simulate the kinetics on all the individually resolved particles in the reactor volume because the computational effort that would be needed. Instead, an Eulerian approach can be chosen to describe the disperse phase as a continuum. The reaction is then calculated as an average of many particles for a given cell volume. While this approach is used less often, it enables the simulation of entire process units and can be a useful tool for designing them. The challenge with this approach is to find the parameters relevant for adsorption, for example to calculate the available surface for adsorption from the particle distribution. Parameters for equilibrium and kinetics are mostly determined experimentally and often depend on many variables. These are therefore often only applicable in specific circumstances. For use in simulations the model should be as broadly applicable as possible.

The goal of this thesis is the formulation of an adsorption model for the Euler-Euler model and to apply it to the lattice Boltzmann method (LBM). The model will include three phases: the continuous phase, the solved adsorbate and the disperse phase (adsorbent). All three are treated as a continuum and the mass transport of the adsorbate to the solid will be modeled. The adsorption model can be validated separately from the particle dynamics and its convergence will be tested. Additionally, a suitable example system has to be found with substances that have known adsorption parameters which are usable for a simulation. Some analytical solutions for different configuration are known and can be used to validate the model at a constant particle density. Afterwards the adsorption model can be coupled with the particle dynamics. The final model will be used to simulate 2D and 3D cases.

Tasks

1. Research
    a. Adsorption
    b. Euler-Euler-Modell
2. Adsorption model
3. Choose system and adsorption parameters
4. Validate adsorption model
5. Coupling with particle dynamics
6. Simulation
7. Validation
8. Documentation

Schedule

Task/Week	1	2	3	4	5	6	7	8	9	10	11	12	13	14	15	16	17	18	19	20	21	22	23	24	25	26
Research																										
Adsorption model																										
Choose system																										
Validate model																										
Coupling with particles																										
Simulation																										
Validation																										
Documentation																										

Vereinbarung

Funktion	Name	Datum	Unterschrift
Bachelorand/Masterrand	Florian Raichle	*04.11.2021*	F. Raichle
Betreuer	Fedor Bukreev	*04.11.2021*	

Declaration of originality

I hereby declare that I have composed this work by myself and without any assistance other than the sources given in my list of works cited. This thesis has not been submitted in the past or is currently being submitted to any other examination institution. It has not been published. All direct quotes as well as indirect quotes which in phrasing or original idea have been taken from a different text (written or otherwise) have been marked as such clearly and in each single instance under a precise specification of the source. I am aware that any false claim made here results in failing the examination.

Karlsruhe, May 23, 2022

Florian Raichle

Contents

Chapter 1
Introduction

Many industries and processes use adsorption as a separation technique for multi-component mixtures. The applications can range from small scale chromatography of proteins [1] to large scale water treatment [2] and petrochemical refinement [3]. For the analysis and optimization of industrial processes, a large simulation domain with complex geometries and fluid flows are often required. At this scale it is impossible to resolve the interface of the particles and fluid and a volume average in some sense is needed [4].

The lattice Boltzmann method (LBM) is gaining interest as an alternative to Navier-Stokes solvers. It has some unique advantages, such as its simple structure and ease of parallelization [5], [6]. While there have been some uses of LBM to simulate adsorption on the pore-scale or on discrete particles [7]–[9], only few examples of the combination of an Euler-Euler approach to particle and adsorption modelling exist. Peng et al. [10], [11] have used LBM to simulate adsorption on clusters of unresolved particles with a constant particle density. Maier et al. [12] have done work on the adsorption on moving particles but with an Euler-Lagrange approach. Ma et al. [13] have chosen a similar approach to the one taken in this thesis in simulating adsorption using volume averaging but with a multiple relaxation time model. Their work was restricted to simpler kinetics, only applied to a fixed bed reactor and did not provide any data as to the convergence of their method. On the other hand, for other NSE solvers there are examples of Euler-Euler models for reactions in fluidized bed reactors [14], [15].

This thesis aims to build on these approaches and combine an Euler-Euler description of moving particles with more detailed adsorption kinetics. It first formulates, then employs an adsorption model based on the linear driving force model with transport equations in the form of the advection diffusion equation for particles, solute and particle loading to form advection diffusion reaction equations. These equations are solved using the lattice Boltzmann method with each component of the model being represented by its own lattice. The fluid is one-way coupled with all the other lattices, which themselves are coupled according to the adsorption model.

The first part of this thesis will introduce the underlying concepts and equations for describing adsorption and fluid dynamics. The chosen adsorption model is explained as well. In the second part the combined advection diffusion reaction equations and the numerical model is shown together with explanations on the implementation of the simulations. The last part shows applications and validations of the model in a series of simulations ranging from a simple batch reactor to the complex flow field in a static mixer.

Chapter 2
Theory

2.1 Adsorption

Adsorption is a complex process with several interacting mechanisms and length scales involved. In short, it describes a mass transfer process between phases. A substance is removed from a liquid and deposited on a solid or the surface of a liquid. The material that provides the surface is called adsorbent and the substance that is deposited is the adsorbate. The amount of deposited substance is called

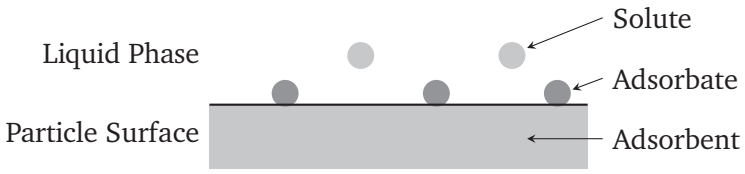

Figure 2.1: Adsorption terminology. Adapted from [16]

particle or adsorbent loading q. The system generally reaches an equilibrium at a certain adsorbent loading and corresponding solute concentration. An equilibrium of course implies that there are in fact two reactions: adsorption, where the adsorbate is accumulating on the surface and desorption, which is the release of the substance from the surface. Both the properties of the surface and the liquid phase affect the process. Concentration, temperature, pH, surface area and porosity are the key factors here [16].

Although adsorption is fundamentally a surface process, the adsorbent uptake is usually measured as a mass related loading q with

$$q = \frac{m_a}{m_A}, \tag{2.1}$$

where m_a is the mass of the adsorbed substance and m_A the mass of the adsorbent. Alternatively q can also be a quotient based on molar concentration using n_a. We will use a mass concentration $C = m_S/V_L$ for the solute concentration as well, where m_S stands for the mass of the solute in solution with the solution volume V_L.

A rigorous theoretical description of adsorption has only been achieved for simple cases like pure gas adsorption. Since this thesis is concerned with adsorption from aqueous solutions, which are even in the simplest case multi-component systems, these theoretical developments will not be expanded upon. For adsorption from liquid solution the adsorbent uptake can only ever be measured relative to the solvent uptake. This makes general prediction of the relevant parameters much more difficult. This fundamental difference, however, does not matter that much in practice and most of the following observations apply to both types of systems [16].

Adsorption in industrial practice is, as a separation process, almost always concerned with multiple components. In this thesis we will focus on single solute systems. Multicomponent systems generally differ in two ways: competitive adsorption changes the equilibrium, which can be accounted for by using multicomponent isotherms, and secondly interactions during mass transport, which necessitates the inclusion of the concentration gradients of all components into the kinetic model.

2.1.1 Adsorption Isotherms

The adsorption equilibrium is characterized using so-called isotherms, which describe the eventual loading q_{eq} of a particle once the equilibrium is reached. This can take several hours to days, depending on the material.

An adsorption isotherm in general is the relationship between the concentration in the fluid phase C and the loading, or $q_{\mathrm{eq}} = f(C_{\mathrm{eq}})$ with $T = \mathrm{const}$. Most commonly this function is determined in batch experiments. There are several models that can be used to describe this relation using differing numbers of parameters [17]. Three of the most common ones have been used in this thesis and are shown in fig. 2.2. The simplest form is simply a constant $q = K$, which corresponds to an irreversible reaction. This may only be applicable for very high concentrations and is only mentioned here for completeness.

Linear Isotherm

The linear relationship between concentration and loading is also called Henry isotherm and relates the loading to concentration by

$$q = KC\,, \tag{2.2}$$

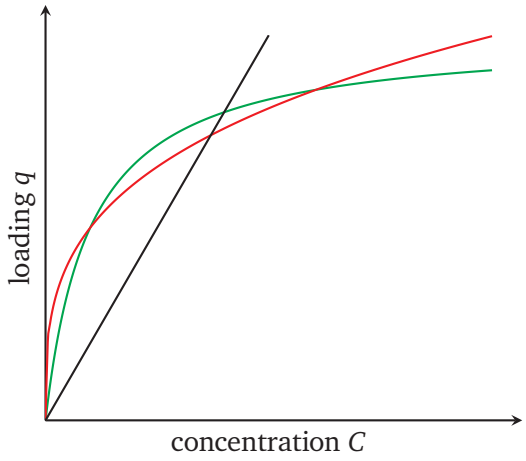

Figure 2.2: Isotherm types: Linear (black), favorable Langmuir(green), Freundlich (red)

with K as the single isotherm parameter often given in L/g.

It can be sufficient for applications with very small concentrations, as it is the limiting case for $C \to 0$ [16]. Additionally, it is useful in model validation, because it enables the formulation of analytical solutions for many models. For this reason it is used in the validation section of this thesis.

Freundlich Isotherm

The Freundlich isotherm is a purely empirical observation, but describes many processes, including many liquid adsorptions systems, fairly well [16]. In this case the loading is

$$q = KC^n\,, \tag{2.3}$$

with the isotherm parameters K and n. Depending on the exponent n, the isotherm can either be favorable ($n < 1$) or unfavorable ($n > 1$). The unit of K depends on the units of C and crucially also n. For this reason, conversion between units for q and C is tricky but certainly possible.

Langmuir Isotherm

A very popular choice is the Langmuir isotherm. It is based on the assumption of a homogenous surface and monolayer adsorption. In the equilibrium we get a loading

$$q = q_m \frac{b\,C}{1 + b\,C} \tag{2.4}$$

with the two constants q_m and b. In the case of adsorption from liquid, unlike in gas adsorption, the parameters q_m and b do not hold any physical significance and are simply fitting parameters.

2.1.2 Adsorption Kinetics

Because reaching equilibrium can take some time, the kinetics play an important role in many processes. Several steps are involved in the adsorption process, the slowest of which will be rate determining [16]:

1. Bulk transport is the usually purely advective transport of the solute to the particle in question. It only depends on the flow field in the reactor and around the particle.
2. Every particle will have a boundary layer around it. The diffusive transport through that film is called film diffusion or external mass transport but should not be confused with the bulk transport in step 1. This is step 1 in fig. 2.3.
3. Intraparticle diffusion is the transport from the surface of the particle to the interior by two different mass transfer mechanisms, pore and surface diffusion. They are steps 2 and 3 in fig. 2.3 respectively.
4. The last step is the actual surface interaction and what we would call the adsorption reaction.

In most cases it is assumed that step one and four are fast enough to be disregarded and only external mass transfer and intraparticle mass transfer are considered [18].

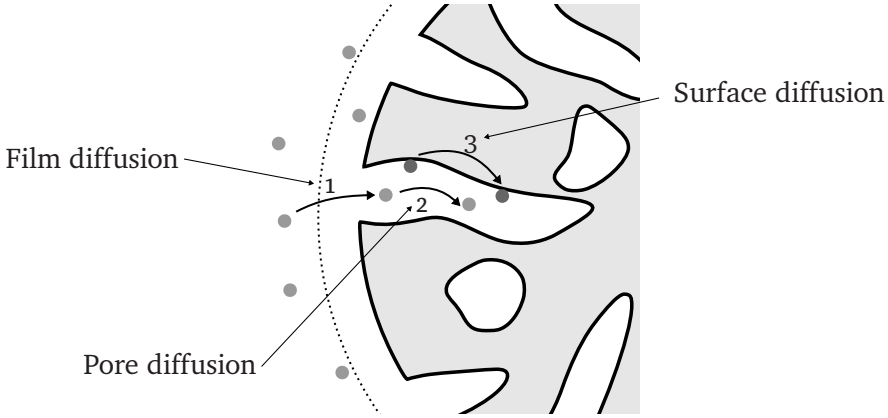

Figure 2.3: Illustration of mass transfer mechanisms. 1: film diffusion, 2: pore diffusion, 3: surface diffusion

Common model assumptions are: constant temperature, completely mixed bulk solution, mass transfer can be described as diffusion process, surface reaction is much faster than diffusion and the adsorbent particles are spherical and identical.

Based on these rate determining steps, equations for the kinetics can be derived. In the simplest case, only one step needs to be included, but combinations are also possible and may result in more accurate models.

Alternatively some empirical rate equations have been proposed and are frequently used in the literature describing adsorbents. Their predictive power, however, is very limited as they can combine several mechanisms in their constants [5], [19], [20]. Their rate constants are usually only applicable to the specific experimental setups they were determined with.

These adsorption rates can be incorporated as a source term into the advection-diffusion equations, as shown by He [21] and Peng [11]. The experimental determination of adsorption kinetic parameters can be difficult, so it is important that we use as few as possible parameters in our model.

Pore Volume and Surface Diffusion Model

The most complete model, which incorporates external mass transfer and intra-particle diffusion, is called Pore Volume and Surface Diffusion Model or PVSDM [22]. The different mass transfer mechanisms that comprise this model are listed in the following sections, as they can be the basis for their own models when a single mechanism dominates.

These models are all based on the description of the adsorption behavior of a single particle, some even taking into account the concentration profile inside the particle.

Film Diffusion

The first step is the transport of the solved adsorbate to the surface of the adsorbent particle, also called external mass transfer. A lower concentration of adsorbate at

the surface C_s causes a gradient that is confined to a layer with thickness δ. Under the assumption of a linear gradient and disregarding all other mass transfer mechanisms, the mass transfer can be determined using Fick's Law:

$$\dot{m}_f = \frac{D_L}{\delta} \frac{A_s}{m_A} (C - C_s) \ . \tag{2.5}$$

The quotient $A_s/m_A = a_m$ is the ratio of surface area to available mass of adsorbent and is a common measure in adsorption. D_L is the diffusion coefficient of the liquid phase, C is the concentration in the liquid phase and C_s is the concentration near the particle surface.

The hydrodynamic conditions in the fluid influence the degree to which film diffusion plays a role. For high fluid velocities, caused for example by increased stirring, film diffusion will become less important and the following transfer mechanisms will dominate [16].

Surface Diffusion

Surface diffusion describes the transport of the adsorbate in the adsorbed state on the internal surfaces or pores of the particle. It takes place in pores that are so small that the adsorbing molecules cannot escape the influence of the pore surface [18]. From Fick's law we get

$$\dot{m}_s = \rho_P D_s \frac{\partial q}{\partial r} \, , \tag{2.6}$$

which can be transformed using a material balance for a spherical particle to

$$\frac{\partial q}{\partial t} = D_s \left(\frac{\partial^2 q}{\partial r^2} + \frac{2}{r} \frac{\partial q}{\partial r} \right) \ . \tag{2.7}$$

Depending on whether film diffusion is considered as well, it can be in series with surface diffusion, which would be reflected in the boundary condition for the concentration at the particle surface.

Pore Diffusion

While surface diffusion takes place on the walls of the pores, pore diffusion refers to mass transport in the pore liquid where the influence of the pore surface can be

neglected [18]. This makes the calculation more difficult as the equilibrium has to be taken into account at every point in the pore system. A simplified equation [16] was found to be

$$\rho_p \frac{\partial q}{\partial t} = D_p \left(\frac{\partial^2 c_p}{\partial r^2} + \frac{2}{r} \frac{\partial c_p}{\partial r} \right) . \tag{2.8}$$

Surface and pore diffusion can be combined into effective diffusion coefficients. For that, either a surface diffusion model or a pore diffusion model is used as the basis and the other mechanism is incorporated as a contribution depending on the isotherm slope. For linear isotherms either approach leads to an identical solution and the two mechanisms can be considered equivalent. [16]

2.1.3 Linear Driving Force Model

Adsorption primarily happens at interfaces and is a heterogeneous reaction and, especially with moving particles, not a bulk phenomenon. This makes it very difficult to describe accurately using an Euler-Euler approach where the particle and interfaces cannot be resolved. We cannot, for example, incorporate a granular representation of the concentration gradients inside every single particle. To work around this issue, Glueckauf and Coates [23] proposed a linearized approach, called linear driving force model (LDF), which is now widely used in adsorption modeling, especially in the description of fixed bed reactors [24], [25].

It postulates an area inside the particle with a linear concentration gradient similar to film diffusion and a core with a spatially constant concentration $\bar{q}(t)$. This is shown in figure 2.4. The model was also derived by Liaw et al. [26], who found that overall this is equivalent to a parabolic concentration profile in the particle. While the model was originally developed to simplify the surface diffusion model it can be extended to include several transfer mechanisms as will be shown below.

The internal mass transport through surface diffusion is

$$\dot{m}_{\text{int}} = \rho_p k_s \left(q_s - \bar{q} \right) , \tag{2.9}$$

with the surface diffusion coefficient k_s and the particle density ρ_p. The surface loading is determined by the isotherm $q_s(t) = f(C_s(t))$. When external mass transfer is not included, $C_s = C$. For spherical particles it was shown [23] that

$$k_s = \frac{5 D_s}{r_p} . \tag{2.10}$$

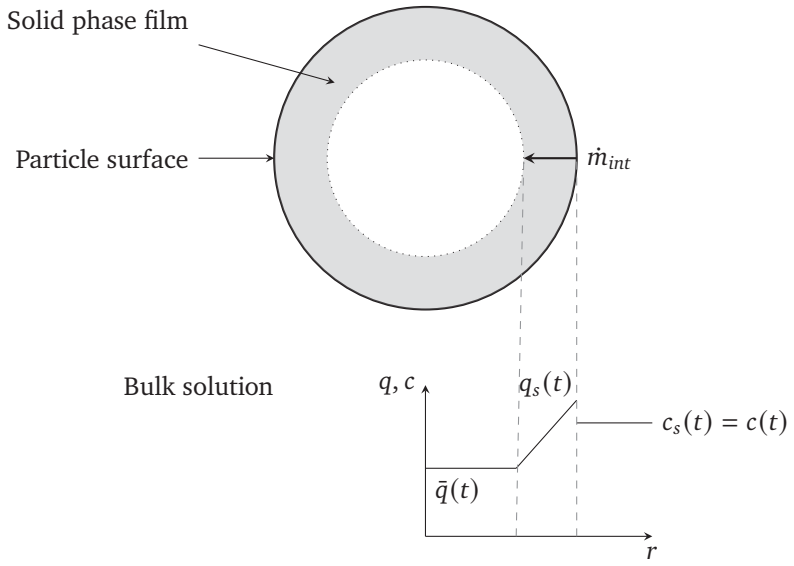

Figure 2.4: Linear concentration profile in particle. Adapted from [16].

The mass balance for a single particle and the surrounding fluid reads

$$\dot{m}_{\text{int}} = \frac{m_A}{A_s}\frac{d\bar{q}}{dt} = -\frac{V_L}{A_s}\frac{dc}{dt}\,. \tag{2.11}$$

When we substitute eq. (2.9) for the mass transport $\dot{m}_{\text{int}}$ in eq. (2.11) we find the mass transfer equation

$$\frac{d\bar{q}}{dt} = k_s\frac{A_s}{V_A}\,(q_s - \bar{q}) = k_s^*\,(q_s - \bar{q})\,. \tag{2.12}$$

For convenience we combine the factors in (2.12) so that

$$k_s^* = k_s\frac{A_s}{V_A} = \frac{15D_s}{r_p^2}. \tag{2.13}$$

Together with the mass balance we can also calculate the change in concentration

$$-\frac{dc}{dt} = k_s^*\frac{\rho_p(1-\varepsilon_B)}{\varepsilon_B}\,(q_s - \bar{q}) \tag{2.14}$$

with the factor $\frac{\rho_p(1-\varepsilon_B)}{\varepsilon_B} = \frac{m_A}{V_L}$ converting the adsorbate loading, which is defined per mass of adsorbent, to concentration, which is defined per volume of liquid. The particle volume is included using the bed porosity ε_B.

If we do not incorporate film diffusion into the model, the surface loading is simply the equilibrium loading corresponding to the bulk concentration:

$$q_s = f(C) \tag{2.15}$$

It has been shown that this model can achieve impressive accuracy while reducing the computational effort [27], [28] which makes it especially useful for numerical simulations. A short comparison between the LDF model and the HSDM can be found in appendix A.

To increase the accuracy of the model further, a variable mass transfer coefficient can be introduced [16]. Using

$$k_s^* = k_{s0}^* \exp \omega \bar{q} \tag{2.16}$$

with the additional empirical parameters ω and k_{s0}^*. These parameters however have to be determined through curve-fitting of experimental data.

Film Diffusion

The model can be extended to include film diffusion on the outside of the particle as well. This configuration is shown in fig. 2.5. The mass flow due to film transfer is

$$\dot{m}_{\text{film}} = k_f \frac{A_s}{m_A} (C - C_s) \ . \tag{2.17}$$

It acts as a boundary condition which we solve to get the surface concentration C_s. With the condition that $\dot{m}_{\text{int}} = \dot{m}_{\text{film}}$ as a basis we get

$$\rho_p k_s (q_s - \bar{q}) = k_f (C - C_s) \tag{2.18}$$

where the surface loading q_s is a function of C_s via the equilibrium. Once the new surface concentration has been found, the corresponding surface loading can be calculated and used as before in eq. (2.12).

Pore Diffusion

The LDF model can also be applied to pore diffusion with some simplifications. By replacing the quotient $\partial q / \partial C$ that occurs in the model with $q_{0,eq}/C_0$, as shown

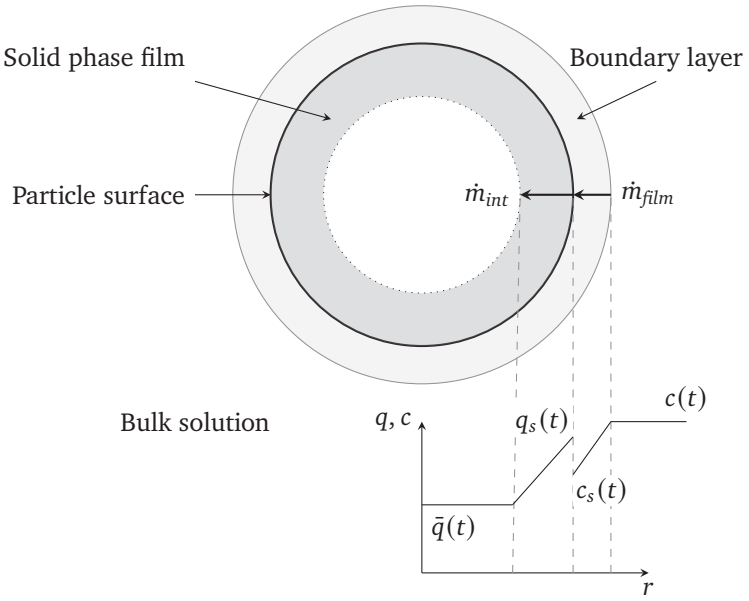

Figure 2.5: Linear concentration profile in particle with film diffusion. Adapted from [16].

by [16], [29], an effective mass transfer coefficient can be formulated to include the pore diffusion coefficient.

$$k^*_{s,\text{eff}} = \frac{15 D_s}{r_p^2} + \frac{15 D_p}{r_p^2} \frac{C_0}{\rho_p \, q_{0,eq}} \tag{2.19}$$

Here C_0 denotes the inlet solute concentration and $q_{0,\text{eq}}$ the corresponding equilibrium loading. This new coefficient can be substituted in eq. (2.12) and (2.14) in cases where pore and surface diffusion both contribute significantly.

Cyclical Adsorption

The LDF model uses a very simple equation for the mass transfer coefficient k_s. It has been shown that this assumption is not always valid for cyclical processes with short cycle times [30], [31]. The cause for this are the assumptions made about the linear concentration profile inside the particle. This will lead to desorption being underestimated [32].

Dominating film diffusion, on the other hand, will reduce the influence of cyclicality because it is independent of the concentration profile inside the particle.

2.1.4 Reaction Kinetics

Experimental data is very often fitted with empirical reaction kinetic models [16], [33]. While they can produce well fitting results, these models do not directly allow any mechanistic insight. They rely only on fitting parameters, which are often only valid for a specific experimental setup [16]. The most common ones are called pseudo-first-order and pseudo-second-order kinetics [34], [35]. They are based on the difference between the equilibrium loading and the current loading of the particle. The first order equation is

$$\frac{d\bar{q}}{dt} = k_1 \left(q_{\mathrm{eq}} - \bar{q}\right) \tag{2.20}$$

and the second order

$$\frac{d\bar{q}}{dt} = k_2 \left(q_{\mathrm{eq}} - \bar{q}\right)^2 . \tag{2.21}$$

The equations are similar to the linear driving force model, the difference however is in the driving force. The equilibrium loading q_{eq} is the final particle loading of the experiment and therefore a constant. The surface loading used in the linear driving force model is dependent on time.

2.1.5 Parameter Estimation

In most cases adsorption parameters cannot be predicted. Experiments have to be conducted, and the parameters can then be determined by using an appropriate model and fitting techniques.

Isotherm parameters are usually determined in batch experiments by measuring the concentration at different points in time and then the adsorbed amount is calculated with a mass balance. The isotherm parameters are determined by fitting an appropriate isotherm model. Attempts at predicting isotherms using, amongst others, potential theory have been made, but their predictive power is often limited. [16]

If we want to model adsorption kinetics in a wide spectrum of conditions, we need to separate the influence of different mass transfer mechanism and determine their respective mass transfer coefficients. The film mass transfer coefficient can for example be determined in a short fixed bed reactor, as the film diffusion will be dominant at first. Several empirical correlations also exist, most using the Sherwood number as a function of the Reynolds number *Re* and the Schmidt number *Sc*.

Intraparticle diffusion coefficients for surface and pore diffusion can be determined in batch experiments by applying the linear driving force model and calculating an average value of k_s^* from the change in concentration dC/dt. Worch [28] also gives an empirical correlation for the adsorption of micropollutants onto activated carbon. For other systems, different correlations would be needed.

2.1.6 Batch Reactor Model

The simplest reactor for adsorption is a batch reactor. The differential mass balance reads

$$m_A \frac{d\bar{q}}{dt} = -V_L \frac{dC}{dt} \,. \tag{2.22}$$

Integration with the initial conditions $C(0) = C_0$ and $\bar{q}(0) = 0$ leads to

$$\bar{q}(t) = \frac{V_L}{m_A} \left(C_0 - C(t)\right) \tag{2.23}$$

We can visualize this as an operating line as seen in fig. 2.6 with the term $-V_L/m_A$ as the slope.

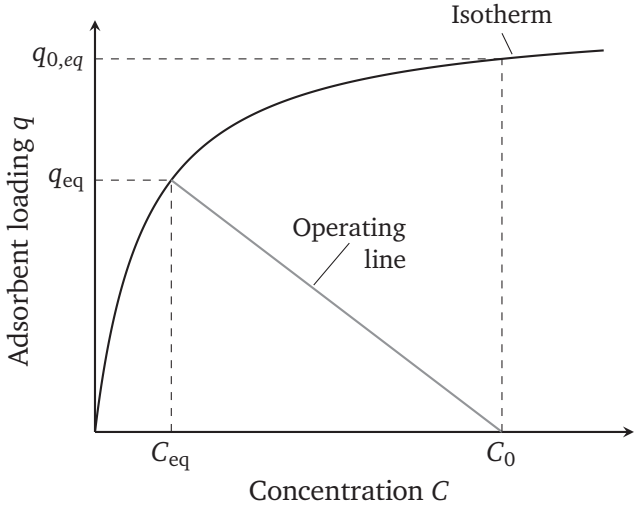

Figure 2.6: Operating lines in a batch reactor and a fixed bed reactor.

Together with the mass transfer equations for dC/dt and $d\bar{q}/dt$, that were derived by looking at a single particle, the equilibrium relationship $q = f(C)$ and initial conditions this system of equations is complete. It can usually only be solved numerically, except for the case of a linear equilibrium, where an analytical solution

exists. The application of the single particle kinetics to the batch reactor assumes homogenous particles and conditions in the volume element.

In summary, when using the LDF model, the system of equations is as follows

$$\begin{aligned} \frac{d\bar{q}}{dt} &= k_s^* \left(q_s - \bar{q}\right) \\ -\frac{dc}{dt} &= k_s^* \frac{(1-\varepsilon_B)}{\varepsilon_B} \rho_p \left(q_s - \bar{q}\right) \\ \rho_p k_s (q_s - \bar{q}) &= k_f (C - C_s) \\ q_s &= f(C_s) \\ \bar{q}(t=0) = 0, \quad & C(t=0) = C_0 \end{aligned} \tag{2.24}$$

The third equation only applies when film diffusion is included. This system of equations is also the basis for the discretized model where each node at each time step can be thought of as a small batch reactor.

2.1.7 Fixed Bed Reactor Model

In a fixed bed reactor the adsorbent is usually in granular form and is packed in a porous bed. During operation, solute of a certain concentration is introduced at the inlet and a steady flow is maintained. The solute travels from the inlet through the column and accumulates on the adsorbent particles until equilibrium is reached. A distinct concentration front forms as initially all the adsorbate can be removed from the solution, leading to a much lower concentration in most of the bed than at the inlet. Only after enough adsorbate has accumulated on the particles and the reaction slows down, does the concentration increase downstream. The velocity of this concentration front is much slower than that of the fluid and depends (in the ideal case) only on the inlet concentration and the amount of adsorbent in the bed.

For adsorption where kinetics play a role, the equilibrium is not reached instantaneously and a characteristic mass transfer zone (MTZ) can be observed. Its shape depends both on the kinetics and the equilibrium [23]. An example can be seen in figure 2.7. The progress of the center of mass of the MTZ, however, will still only depend on the equilibrium.

There are three stages that every particle experiences, which can be seen as more or less distinct zones. These are shown in fig 2.7 as well. Zone I is simply an unloaded bed with $C = 0$ and usually an initial loading $q(t = 0) = 0$. The second zone is the

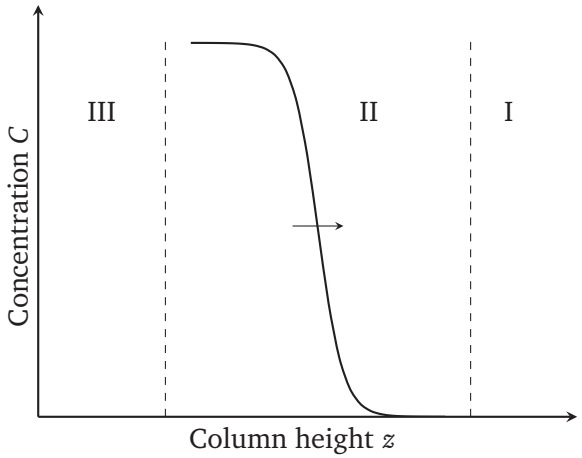

Figure 2.7: Concentration profile with MTZ in a fixed bed adsorber

MTZ where the mass transfer takes place and the concentration rises. In the third zone, which is closest to the inlet, the particles are already saturated and no net mass transfer takes place. Therefore, the solution still has its initial concentration. The time it takes for the center of mass of the MTZ to reach the outlet is called ideal breakthrough time t_b^{id}. The balance equation in the ideal case of instantaneous equilibrium is

$$C_0 \dot{V} t_b^{id} = q_0 m_A + C_0 \varepsilon_B V_R \,, \tag{2.25}$$

with V_R as the reactor volume. This gives us the ideal breakthrough time as

$$t_b^{id} = \frac{q_0 \, m_A}{C_0 \dot{V}} + \frac{\varepsilon_B \, V_R}{\dot{V}} = t_{\mathrm{st}} + t_r \,, \tag{2.26}$$

which can be split into the stoichiometric time t_{st} and the residence time t_r. If $t_{\mathrm{st}} \gg t_r$, the residence time can be neglected [16]. By substituting the column height h using $V_R = h\rho_B$ we can derive the velocity of the MTZ with

$$v_{\mathrm{MTZ}} = \frac{h}{t_b^{id}} = \frac{C_0 \dot{V} / A_R}{q_0 \rho_B + C_0 \varepsilon_B} \,. \tag{2.27}$$

For favorable isotherms a self-sharpening effect can be observed [23]. This means that even an initially flattened concentration front would become vertical again.

The adsorption behavior in fixed bed columns is usually analyzed using so-called breakthrough curves (BTC). These are constructed by measuring the outlet concentration over time and are just a mirrored concentration profile (see sect. 4.2) but much easier to measure. The axes are related through the travelling velocity of the MTZ. Apart from the general shape there are two values that are used to analyze the

breakthrough behavior. The first is the real breakthrough time t_b, which is the time at which the outlet concentration first rises and the second is the stoichiometric time t_{st} as an approximation of the ideal breakthrough time.

Diffusion, amongst other factors, leads to a phenomenon called axial dispersion in fixed bed reactors. It will lead to a spreading of the MTZ and therefore a flatter breakthrough curve. Many models, including many implementations of the LDF, do not include this term. It is however important to keep in mind because we use the advection diffusion equations and diffusion cannot be entirely disregarded. There are ways to include the dispersion in the film diffusion coefficient [36] to account for this phenomenon in a model.

2.2 Fluid Dynamics

The goal of this thesis is the coupling of fluid dynamics and adsorption dynamics. Therefore, in addition to the adsorption model, we also need a model for the fluid dynamics. All components in the system are described by an Euler approach. They can be described by continuity, momentum and species balances, depending on the type of the transported component.

2.2.1 Navier-Stokes Equations

The equations for mass and momentum that describe the fluid, namely the Navier-Stokes equations (NSE), are the following.

$$\frac{\partial \rho}{\partial t} + \nabla \cdot (\rho \boldsymbol{u}) = 0 \tag{2.28}$$

This represents the compressible continuity equation with the density ρ and the fluid velocity $\boldsymbol{u}$.

The momentum equation is

$$\frac{\partial \rho \boldsymbol{u}}{\partial t} + (\rho \boldsymbol{u} \cdot \nabla)\boldsymbol{u} = -\frac{1}{\rho}\nabla p + \mu \nabla^2 \boldsymbol{u} + \boldsymbol{F}\,, \tag{2.29}$$

with the pressure p, the viscosity μ and a force $\boldsymbol{F}$. This single equation in Einstein notation stands for up to three equations, one for every dimension of the problem. These equations represent the compressible NSE.

Often the assumption $\rho = \text{const.}$ is made, which leads to the incompressible variants of the continuity equation

$$\nabla \cdot \boldsymbol{u} = 0 \tag{2.30}$$

and the momentum equation

$$\frac{\partial \boldsymbol{u}}{\partial t} + (\boldsymbol{u} \cdot \nabla)\boldsymbol{u} = -\frac{1}{\rho}\nabla p + \nu \nabla^2 \boldsymbol{u} + \boldsymbol{F}\,, \tag{2.31}$$

now with the kinematic viscosity ν. The LBM actually solves a weakly compressible NSE [5] because density is in fact variable.

To close the system of equations, we also need an equation of state. A common example for fluids is the isothermal equation of state

$$p = \rho R T_0 = \rho c_s^2\,, \tag{2.32}$$

with c_s as the speed of sound.

Volume Averaged Navier Stokes Equations

In order to describe dense particle flows more accurately without having to deal with the particle-fluid interface in detail, an averaging procedure can be employed. This achieves a two-way coupling between the fluid and the particles. The basic idea is to find equations describing the relevant fluid properties in a volume around an arbitrary point in space **x** with the averaged influence of particles included. To that end an averaging operator $\langle \cdots \rangle$ is introduced. Following Whitaker[37] and Enwald[38], the volume average is used:

$$\langle \cdots \rangle = \frac{1}{V_f} \int_{\mathrm{V_f}} \cdots \, dV\,. \tag{2.33}$$

Both an intrinsic and a superficial average are used with the porosity as a conversion factor. As an example, the superficial average over just the volume of fluid, indicated by a phase indicator function χ, is the fluid volume fraction ε:

$$\langle \chi \rangle = \varepsilon\,. \tag{2.34}$$

The phase indicator function $\chi(x)$ for the phase A is 1 if $x \in A$ and 0 otherwise.

Applying the procedure to the NSE, the resulting volume averaged equations (VANSE) are as follows [38], [39].

$$\frac{\partial \varepsilon \rho}{\partial t} = \nabla \cdot (\varepsilon \rho \langle \boldsymbol{u} \rangle) \tag{2.35}$$

$$\frac{\partial \varepsilon \rho \langle \boldsymbol{u} \rangle}{\partial t} + (\varepsilon \rho \langle \boldsymbol{u} \rangle \cdot \nabla) \langle \boldsymbol{u} \rangle = -\varepsilon \nabla \langle p \rangle + \mu \nabla^2 (\varepsilon \langle \boldsymbol{u} \rangle) + \varepsilon \boldsymbol{F} \tag{2.36}$$

The force term $\boldsymbol{F}$ includes amongst body forces also an additional term that represents the back coupling from the particles and which has to be modelled [40]. Volume averaging of the ADE works similarly but without any new forcing tems [41], [42].

2.2.2 Solute

The dissolved adsorbate is described by its own species mass balance [14], [15] in the advection diffusion reaction equation (ADRE)

$$\frac{\partial C}{\partial t} + \nabla \cdot (C \boldsymbol{u}) = \nabla \cdot (D \nabla C) + s \tag{2.37}$$

with C as the concentration and s as a source term. It combines an advective component in the second term on the left-hand side and a diffusive term on the right-hand side with the diffusion constant D.

The source term $s = \dot{m}_{\text{ads}}$ comes from the change dC/dt in a volume element as introduced in section 2.1.6.

The ADRE has a very similar structure as the incompressible NSE with

$$\rho \boldsymbol{u} \rightarrow C, \quad \rho \boldsymbol{u}\boldsymbol{u} + p\boldsymbol{I} \rightarrow C\boldsymbol{u}, \quad \nu \rightarrow D, \quad \boldsymbol{F} \rightarrow s \tag{2.38}$$

which makes it a great candidate to be solved by the lattice Boltzmann method as well.

2.2.3 Particles

Particle density

The moving adsorbent particles are described by the advection diffusion equation, meaning they are not resolved individually but represented by a particle concentration $\rho_B(x)$. The symbol of ρ_B is rooted in the common usage of bulk density in

adsorption literature, which is the same as a particle concentration, although usually not treated as a transportable property. The advection diffusion equation (ADE) for the particles is

$$\frac{\partial \rho_B}{\partial t} + \nabla \cdot \left(\rho_B \boldsymbol{u}_p\right) = \nabla \cdot (D \nabla \rho_B) + \boldsymbol{F}\,, \tag{2.39}$$

where D is a diffusion coefficient, $\boldsymbol{u}_p$ the particle velocity and $\boldsymbol{F}$ a force term. We use ρ_B as a measure of mass of particles per volume of flow, as opposed to ρ_p, which is the material density of the particles. Their motion is coupled to that of the fluid through the fluid velocity $\boldsymbol{u}_f$ which is calculated using the NSE. While for very small particles it is reasonable to simply use the fluid velocity as the particle velocity, another approach is the use of a force term $\boldsymbol{F}$ that depends on the fluid velocity to calculate the particle velocity. One choice for the force term is for example Stokes' drag force [43] with

$$\boldsymbol{F}_{\text{St}} = 6\pi\rho\nu r_p(\boldsymbol{u}_f - \boldsymbol{u}_p) \tag{2.40}$$

where $\boldsymbol{u}_f$ is the fluid velocity and $\boldsymbol{u}_p$ the particle velocity.

Particle loading

In addition to the particle density we also track the particle loading $\bar{q}$, as described in section 2.1.3 with

$$\frac{\partial \bar{q}}{\partial t} + \nabla \cdot (\bar{q}\boldsymbol{u}) - \nabla \cdot (D \nabla \bar{q}) = \rho_p \, \dot{m}_{\text{ads}}\,. \tag{2.41}$$

Here we also have a source term $\dot{m}_{\text{ads}}$ that represents the change in loading from adsorption. It is the same as the source term in the solute transport equation but with an additional factor of the particle density, since the loading is spread amongst the particles.

The inclusion of diffusion for the particles makes the model a dispersive one. The coefficient D can include contributions from different mechanisms, such as diffusion, mixing etc. This makes it possible to be solved using the lattice Boltzmann method. Depending on the particle size it may be more desirable to have no diffusion at all. This can only be approximated by a very small diffusion coefficient D. How this can be acheived will be picked up again in section 3.3.4.

Chapter 3
Model

3.1 Dimensionless Quantities

Dimensionless quantities are a useful tool in engineering, especially when comparing systems of different scales or materials. In the following sections, the dimensionless quantities that can be used to describe adsorption systems as encountered in this thesis are introduced.

Reynolds Number

Arising from the NSE through non-dimensionalization, the Reynolds number

$$Re = \frac{uL}{\varepsilon_B \nu} \tag{3.1}$$

is the quotient of inertial forces to viscous forces. It contains the fluid velocity u, a characteristic length L, the dynamic viscosity ν and optionally the bed porosity ε_B. It can be used to gauge whether the flow is laminar or turbulent.

Care has to be taken when choosing the characteristic length L. Because the choice is in principle arbitrary, it can differ between types of flows and publications. A common definition for flow in a pipe, for example, is the diameter of the pipe and for flow in porous media the particle diameter is often used.

Schmidt Number

The Schmidt number

$$Sc = \frac{\nu}{D_L}\,, \tag{3.2}$$

with the fluid viscosity ν and the diffusion constant D_L of a particular solute in the fluid describes the relative importance of momentum diffusivity compared to mass diffusivity. It can be seen as the ratio of the thickness of hydrodynamic layer and the mass-transfer boundary layer.

Péclet Number

The quotient of advective transport and diffusive transport is called Péclet number. For mass transfer it is defined as

$$Pe = \frac{uL}{D_L} = Re\,Sc \tag{3.3}$$

and can be also be formed from the product of the Reynolds number and Schmidt number. The Péclet number is for example used in fixed bed reactors to quantify the influence of axial dispersion on the result. For values over 40 the reactor can be assumed to exhibit plug flow behavior [36].

Sherwood Number

Estimation of film mass transfer coefficients is often done using the Sherwood number Sh. It is the quotient of the convective diffusion rate and the diffusion rate

$$Sh = \frac{k_f d_p}{D_L}\,. \tag{3.4}$$

Several equations exist to correlate the Sherwood number with the Reynolds and Schmidt numbers. An overview of the many correlations can for example be found in Worch [16].

Biot Number

The Biot number, originally defined for heat transfer problems, can also be used for mass transfer. In this case it is defined as

$$Bi = \frac{k_f r_p C_o}{D_s \rho_p q_e} \tag{3.5}$$

and describes the ratio of surface diffusion and film diffusion. If it is larger than 50, film diffusion is negligible, for $Bi < 0.5$ film diffusion is dominant [16].

3.2 Adsorption Model

As previously mentioned, we use an Euler-Euler approach to describe the different components in the model. The equations for the particle and species transport are the advection diffusion equations with an added source term. They resemble the NSE in structure and can be solved with an adapted lattice Boltzmann method as shown in [40].

The source term which models the adsorption process stems from the mass equation of the adsorption model. We have chosen the linear driving force model for the numerical calculations primarily because of its simplicity. The main advantage is that, because no concentration gradients inside the particle are involved in the model, a single quantity describing the state of the particle is sufficient. This makes it easily applicable to the Euler-Euler approach with moving particles, where this single quantity can be transported. The other quantity in the model, surface loading, can be calculated for each time step from the surrounding fluid.

The combination of the ADE and adsorption source terms for the linear driving force model results in the following equations. Without film diffusion:

$$\begin{aligned} \dot{m}_{\text{int}} &= \frac{3k_s}{r_p}\left(\rho_B q_s - C_{\bar{q}}\right) , \\ \frac{\partial C}{\partial t} + \nabla\cdot(C\boldsymbol{u}) &= \nabla\cdot(D_e\nabla C) - \frac{1}{\varepsilon}\dot{m}_{\text{int}} , \\ \frac{\partial C_{\bar{q}}}{\partial t} + \nabla\cdot\left(C_{\bar{q}}\boldsymbol{u}_p\right) &= \dot{m}_{\text{int}} , \\ q_s &= f(C_s) , \\ C_s &= C , \end{aligned} \tag{3.6}$$

where $C_{\bar{q}}$ denotes the particle loading per volume of fluid as opposed to per mass of adsorbents as it is usually done when the mass of the available adsorbent is constant. The conversion is simply $C_{\bar{q}} = \rho_B\bar{q}$. This is done because the model includes the transport of adsorbed mass by moving particles, so using a volumetric mass density is more appropriate. The factor to convert from reactor volume to adsorbent volume $1/\varepsilon$ is only implemented when using the VANS equations.

The last equation in (3.6) is the boundary condition for C_s in the case of no film diffusion. With film diffusion we replace the boundary condition for C_s with

$$k_s(\rho_B q_s - C_{\bar{q}}) = k_f(C - C_s) . \tag{3.7}$$

If external mass transfer is included, the boundary condition for the surface concentration and loading has to be solved numerically, since it is implicit. The Newton method has been used in literature [44] to solve this, a C++ implementation of MATLAB's *fsolve* function [45] is used in this thesis.

The coupling of the different lattices and equations is shown in fig. 3.1. Hexagons

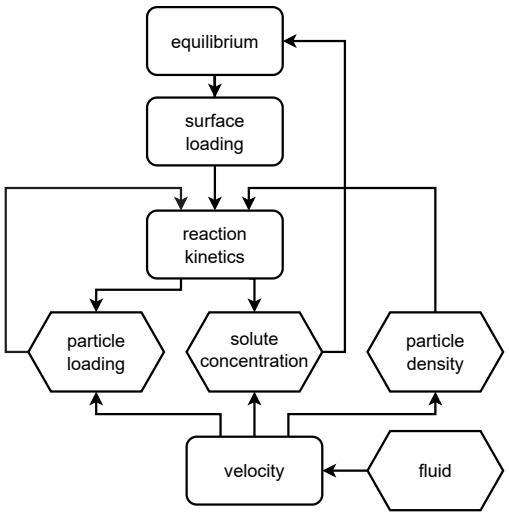

Figure 3.1: Adsorption model flow diagram

mark the four different lattices used in the model and the rounded rectangles stand for the equations or quantities involved. The top part depicts the adsorption coupling and the lower part the velocity coupling.

3.2.1 Nondimensionalization

The adsorption equations can be converted to a dimensionless form. In some cases this makes it possible to find analytical solutions. We define the dimensionless concentration X and loading Y using the inlet concentration C_0 and the corresponding equilibrium loading $q_{0,\mathrm{eq}}$ as

$$X = \frac{C}{C_0}, \quad Y = \frac{q}{q_{0,\mathrm{eq}}}\,. \tag{3.8}$$

The dimensionless Freundlich isotherm is then

$$Y = X^n\,, \tag{3.9}$$

and the Langmuir isotherm

$$Y = \frac{X}{R + (1 - R)X}\,, \tag{3.10}$$

with the separation factor

$$R = \frac{X(1-Y)}{Y(1-X)} = \frac{1}{1 + b\,C_0}\,. \tag{3.11}$$

We can also apply the separation factor to the Freundlich isotherm and get

$$R = \frac{X^{1-n} - X}{1 - X} \tag{3.12}$$

which now depends on the concentration X. For adsorption models in which a constant R is assumed, a mean value has to be used.

Using these dimensionless quantities, the mass balance now reads

$$X + D_b\,\bar{Y} = 1\,, \tag{3.13}$$

with the distribution factor

$$D_b = \frac{m_A\,q_{0,\mathrm{eq}}}{V_L\,C_0} \tag{3.14}$$

and the mass transfer equation

$$\frac{d\bar{Y}}{dT} = Y_s - \bar{Y}\,. \tag{3.15}$$

These equations are used for the analytical solutions. For the simulation we have to rely on the original equations, because the time step of the adsorption equations has to match that of the fluid simulation. The conversions done there are explained in section 3.4.

3.3 Lattice Boltzmann Model

The equations in chapter 2 can in principle be solved numerically by a number of different methods. For this thesis the lattice Boltzmann method was chosen. It recovers the Navier-Stokes equations but using a different approach than traditional solvers and is a so-called mesoscopic approach, as it deals with particle populations

which can be understood to lie in between the macroscopic NSE and the microscopic particle kinetics. Instead of solving the NSE directly, it numerically solves the Boltzmann equation. The macroscopic NSE can be recovered in a separate step.

The unique approach behind the LBM is the discretization in space, time and velocity space. The discrete velocity distribution function $f_i(\boldsymbol{x}, t)$ can be thought of as a particle density function for particles with discrete velocities, also called populations. Only a certain set of velocities $\boldsymbol{c}_i$ is allowed which all lead to neighboring lattice nodes. They are chosen so that a particle would travel from one node to the next in exactly one time step. Starting with the Boltzmann equation and after discretization of space, time and velocity we get

$$f_i(\boldsymbol{x} + \boldsymbol{c}_i \Delta t, t + \Delta t) = f_i(\boldsymbol{x}, t) + \Omega_i(\boldsymbol{x}, t)\Delta t\,, \tag{3.16}$$

with the collision operator $\Omega_i(\boldsymbol{x}, t)$. This is known as the lattice Boltzmann equation.

This equation only deals with populations, but we also need to recover the macroscopic quantities. They can be calculated by taking moments of the distribution functions. The zeroth moment gives density and the first moment gives momentum:

$$\rho = \sum_i f_i \qquad\qquad \rho u = \sum_i \boldsymbol{c}_i f_i\,. \tag{3.17}$$

The second moment is defined as

$$\boldsymbol{\Pi} = \sum_i \boldsymbol{c}_i \boldsymbol{c}_i f_i$$

and is related to the stress tensor.

Analysis of the LBM through a Chapman-Enskog expansion and comparison with the NSE reveals that the Navier-Stokes equations can indeed be recovered with the viscosity being connected to the relaxation time τ of the collision operator by

$$\nu = c_s^2 \left(\tau - \frac{\Delta t}{2}\right) \tag{3.18}$$

with c_s as the speed of sound. [5] The equation of state for the LBE is $p = c_s^2 \rho$.

The structure of eq. (3.16) lends itself to the separation into a streaming step and a collision step. This is also how most solvers are implemented. The populations

are propagated to neighboring nodes according to their velocities in the streaming step, this is represented by the left-hand side of (3.16). In the collision step new population densities are calculated using the collision operator. This step can usually be a local operation, meaning no neighboring nodes need to be accessed. The LBM is therefore easily parallelized.

BGK-Collision Operator

An important contribution to recovering physical behavior is the collision operator. Using the fairly simple BGK operator the NSE can be recovered. It is defined as

$$\Omega_i = -\frac{f_i - f_i^{eq}}{\tau} .$$

This collision operator can be viewed as a relaxation of the populations f_i towards an equilibrium given by

$$f_i^{eq}(\boldsymbol{x}, t) = w_i \rho \left(1 + \frac{\boldsymbol{c_i} \cdot \boldsymbol{u}}{c_s^2} + \frac{(\boldsymbol{u} \cdot \boldsymbol{c}_i)^2}{2c_s^4} - \frac{\boldsymbol{u} \cdot \boldsymbol{u}}{2c_s^2} \right) .$$

The rate of relaxation is given by the relaxation time τ. Weights w_i are used, which are specific to each velocity set. The macroscopic variables that are included in the equilibrium are computed according to eq. (3.17). An important property of the equilibrium is that its moments are the same as those of the populations f_i themselves.

Other operators, like TRT (two relaxation times) and MRT (multiple relaxation times) are available and can bring accuracy and stability improvements.

Discretization and Lattice Units

LBM uses a square lattice with the lattice spacing Δx. Most commonly lattice units are used in the simulation, where $\Delta x^\star = \Delta t^\star = 1$. This has the advantage of also making the problem dimensionless, which is always recommended for fluid simulations. The chosen conversions may however be different from conventional NSE solvers. Three conversion factors denoted by C are needed to form a valid unit system. All other conversions can be derived from those. Commonly we set $\Delta x^\star$, $\Delta t^\star$ and $\rho^\star$ to unity and get the conversion factors

$$C_l = \Delta x, \quad C_t = \Delta t \quad \text{and} \quad C_\rho = \rho \, . \tag{3.19}$$

The lattice relaxation time $\tau^\star$ is related to the relaxation time by $\tau = C_t\,\tau^\star$. In most cases the lattice relaxation time is used in the following sections, especially when listing actual values, but the star notation has been omitted.

Velocity Sets

The velocity space in LBM is discretized with a set of velocities $\boldsymbol{c}_i$. The nomenclature for these sets usually follows the scheme of $DdQq$ with d denoting the number of spatial dimensions and q the number of discrete velocities. Several sets are available, depending on the application. They represent discrete directions in which particles can move.

For example, the *D3Q7* velocity set includes the directions perpendicular to the faces of a cube with the lattice node at its center plus the zero velocity. In this case we would need two sets of weights w_i, one for the zero velocity and one for all the others, since their vectors have the same length. Other common velocity set for two dimensions are *D2Q9* and *D3Q19* for 3D. In these cases there are several sets of weights, as the velocity vectors are of different lengths.

There is a trade-off between computational cost and accuracy, both increase for larger sets. For advection diffusion we can actually use fewer velocities, which is why *D3Q7* is used in this thesis.

The speed of sound depends on the velocity set and for most $c_s^\star = \sqrt{1/3}$. However, for the lattice *D3Q7* it is different from the standard with $c_{s,\mathrm{ADE}}^\star = \sqrt{1/4}$.

3.3.1 Advection Diffusion

The discretization of the advection diffusion reaction equation follows the example of the NSE, which can easily be justified by their very similar forms. Following the same discretization procedure we get

$$g_i(\boldsymbol{x} + \boldsymbol{c_i}\Delta t, t + \Delta t) - g_i(\boldsymbol{x}, t) = \Omega_i(\boldsymbol{x}, t) + \Delta t\, S_i(\boldsymbol{x}, t)\,, \tag{3.20}$$

where S_i is a suitable source term that fulfills the condition $\sum_i S_i = s$.

The collision operator Ω_i also follows the BGK approach

$$\Omega_i = -\frac{1}{\tau}\left(g_i - g_i^{eq}\right)\,,$$

with the equilibrium defined as

$$g_i^{\mathrm{eq}} = w_i C \left(1 + \frac{\boldsymbol{c}_i \cdot \boldsymbol{u}}{c_s^2} + \frac{(\boldsymbol{c}_i \cdot \boldsymbol{u})^2}{2c_s^4} - \frac{\boldsymbol{u} \cdot \boldsymbol{u}}{2c_s^2}\right) \tag{3.21}$$

with the concentration C.

Instead of the viscosity, we have the diffusion coefficient D which is defined similarly:

$$D = c_s^2 \left(\tau_g - \frac{\Delta t}{2}\right) . \tag{3.22}$$

The concentration can be obtained from the zeroth moment of the advection diffusion equations [46]

$$C = \sum_i g_i . \tag{3.23}$$

This is the only moment that is conserved, momentum is not, so the velocity has to be calculated using the NSE, or LBE in our case. For this reason a lattice with only a few discrete velocities is sufficient but often higher isotropy lattices are used anyway [5].

With the addition of a source term, some redefinitions have to be made. A Chapman-Enskog analysis reveals an unwanted term [47] that can be eliminated by setting

$$C = \sum_i g_i + \frac{S_i \Delta t}{2} \quad \text{and} \quad S = \left(1 - \frac{1}{2\tau_g}\right) w_i s \tag{3.24}$$

similarly to the approach used for the LBE with a force term [48].

3.3.2 Boundary Conditions

Boundary conditions are required in all attempts to solve differential equations. First the general types of boundary conditions are introduced and afterwards their specific implementations for the LBM are shown.

First Order

A first order boundary condition, also known as Dirichlet boundary condition, sets the missing value y according to some function f:

$$y = f\,. \tag{3.25}$$

In the context of thermal advection diffusion this is also called temperature boundary. The equivalent in our case is concentration. This type is often used at inlets.

Second Order

Instead of the value itself, the Neumann boundary condition sets the normal derivative at the boundary:

$$\frac{\partial y}{\partial n} = f\,. \tag{3.26}$$

In thermal advection diffusion this is called a heat flux boundary. For advection diffusion concerned with mass transport, a Neumann boundary sets mass transport through diffusion to zero, but does not affect advection [49].

Lattice Boltzmann boundaries

The lattice Boltzmann method poses some unique challenges when it comes to boundaries. In general the aim is to find values for the undefined populations that are entering the domain. One of the simplest boundary implementations is called bounce back, where the outgoing populations are simply used as incoming populations. This results in a no-slip boundary.

A periodic boundary is realized by using the populations that exit at one side of the domain as the entering populations on the other side.

A velocity boundary can be implemented using a bounce back approach with an additional term that includes the velocity at the wall $\boldsymbol{u}_w$:

$$f_i(\boldsymbol{x}_b, t + \Delta t) = f_i^*(\boldsymbol{x}_b, t) - 2w_i\rho_w\frac{\boldsymbol{c}_i\boldsymbol{u}_w}{c_s^2}\,, \tag{3.27}$$

where $\boldsymbol{x}_b$ is the boundary node's position.

Pressure boundaries can be realized with an anti-bounce-back approach where the sign of bounced back populations is changed [5]. The equation has a similar structure as the velocity boundary. The difficulty here lies in the estimation of the density ρ_w and the velocity $\boldsymbol{u}_w$.

3.3.3 Accuracy

Different error sources contribute to the overall error of a simulation. An obvious error in any discretized equation is the truncation error, which should tend to zero when Δx and Δt go towards zero. In a stable system this should also dictate the order of convergence. Generally the LBM is second order accurate in respect to both temporal and spatial discretization [5], [50].

One important property of the LBM is the relation of the viscosity with the lattice relaxation time and discretization steps

$$\nu = c_s^{\star 2} \left(\tau^\star - \frac{1}{2} \right) \frac{\Delta x^2}{\Delta t} , \tag{3.28}$$

which means that viscosity can influence the accuracy of the BGK model.

Multiple other error terms can contribute to the overall error, such as modelling errors. One example is the compressibility error, which scales with

$$O(Ma^2) \propto 1/c_s^2 \propto \Delta t^2 / \Delta x^2 . \tag{3.29}$$

Another is the BGK truncation error, which scales with $(\tau - 1/2)^2$. [5]

Convergence & Scaling

The main tool to assess the accuracy of discretized equations is the convergence towards the solution measured as the experimental order of convergence (EOC). It is easier than determining the formal truncation error and is done by reducing Δt and Δx successively and measuring the error to a given solution.

The obvious approach is to keep $\Delta x \propto \Delta t$, this is called acoustic scaling. Generally, diffusive scaling is used when measuring the order of convergence for LBM. This

is done to keep the compressibility and discretization error of the same order by setting

$$\Delta x^2 \propto \frac{\Delta t^2}{\Delta x^2} \rightarrow \Delta t \propto \Delta x^2 \,, \tag{3.30}$$

which reduces the compressibility and discretization errors simultaneously [51]. This has the consequence of making the LBM effectively first order accurate in time [5].

The EOC can be determined using three numerical solutions ϕ_i for different mesh sizes with a constant scaling factor r. If, for example, the number of points is doubled, r would be 2. The order of convergence is [52]

$$\text{EOC} = \frac{\log\left(\frac{\phi_3 - \phi_2}{\phi_2 - \phi_1}\right)}{\log(r)} \,. \tag{3.31}$$

It can also be estimated by the slope of a line fitted to the error in a double logarithmic plot over the grid number.

Error Calculation

The most common measure of the error between a numerical approximation q_n and the known solution q_a is the so called $\mathcal{L}_2$ error norm. The relative error is then calculated as follows:

$$\frac{\|q_n - q_a\|_2}{\|q_a\|_2} = \sqrt{\frac{\sum_x \left(q_n(x,t) - q_a(x,t)\right)^2}{\sum_x q_a^2(x,t)}} \,. \tag{3.32}$$

3.3.4 Stability

The fact that the relaxation time and viscosity or diffusivity, depending on the lattice type, are connected, has consequences for stability considerations.

A necessary stability condition for the BGK operator is that $\tau^\star > 1/2$ [5]. There are however several other criteria and boundary conditions which can reduce the stable region considerably. The maximal stable lattice velocity depends on the relaxation time [5] but for $\tau > 1$ the maximum is a constant.

In the case discussed in this thesis the coupling between two types of lattices complicates the choice of parameters. Using the Schmidt number with the definitions of the viscosity and diffusivity in LBM we get

$$Sc = \frac{\nu}{D} = \frac{c^{\star 2}_{s,F}}{c^{\star 2}_{s,\mathrm{ADE}}} \frac{\Delta t_{\mathrm{ADE}}}{\Delta t_F} \frac{(\tau^\star_F - 0.5)}{(\tau^\star_{\mathrm{ADE}} - 0.5)} \,. \tag{3.33}$$

Assuming the same Δt for both lattices, this gives us the matching relaxation times for the ADE and the NSE lattices

$$\tau^\star_{\mathrm{NSE}} = (\tau^\star_{\mathrm{ADE}} - 0.5) \frac{c^{\star,2}_{s,\mathrm{ADE}}}{c^{\star,2}_{s,F}} Sc + 0.5 \,. \tag{3.34}$$

With the values of Sc commonly being up to around 1000, this makes the relation very sensitive to the value of $\tau^\star_{\mathrm{ADE}}$ and values very close to the minimum of 0.5 are often required.

An alternative approach might be the utilization operator splitting or substeps where the fluid lattice has a larger Δt than the advection-diffusion lattice, thereby allowing for more control over stability and accuracy. This has for example been proposed by Micale et al. [14] in their simulation of reaction kinetics in fluidized beds.

3.4 Implementation

The *OpenLB* library already has dynamics implemented for the fluid and ADE with a source term. The values for the source term are computed in a custom coupler at each time step and saved for each lattice node. In the collision step this source term is then included according to eq. (3.20) and eq. (3.24).

The coupling is done as a separate step before collision by a `PostProcessor`. Its job is to get the required values from the different lattices, calculate the source term and write the new values to the lattices. It utilizes the existing implementation of sourced advection diffusion dynamics in *OpenLB*. The flow of information was shown in fig. 3.1

The code was designed to accommodate all the different flavors of the LDF model, such as with and without film diffusion, different isotherms etc. Fig. 3.2 shows the classes that were implemented for this project. Different isotherms can be implemented by inheriting from the `Isotherm` class, as is shown with the `linearIsotherm`.

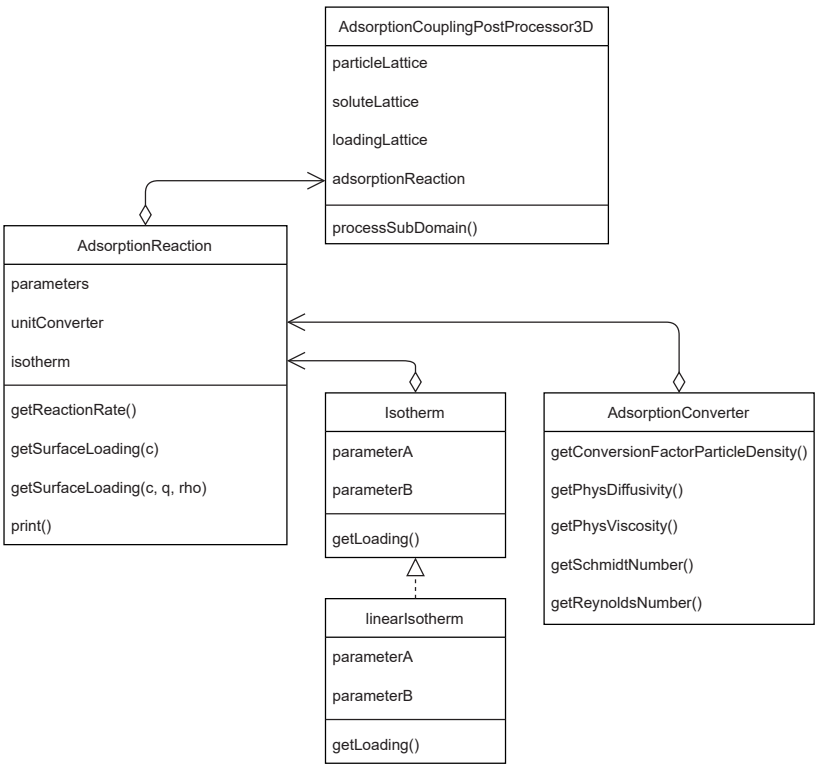

Figure 3.2: UML for classes related to adsorption coupling.

The coupling post processor calls the `getReactionRate()` method in `AdsorptionReaction` which can use either the pure surface diffusion model or a combined film and surface diffusion model by calling two different overriding methods called `getSurfaceLoading()`. These two methods take as parameters either only the solute concentration C or the particle loading q, the particle concentration ρ_B and C.

Due to the fact, that three different lattices with different densities which potentially differ by orders of magnitude need to be coupled, the choice of units and their consistent use is important. A custom `UnitConverter` called `AdsorptionConverter` was therefore implemented. The customary units of the material properties as used in the literature are listed in table 3.1.

Table 3.1: Process parameters

Parameter	Symbol	Unit
Concentration	C	mg/L
Loading	q	mg/g
Density	ρ	kg/m^3
Length	L	m

Because the values for particle and solute concentration and loading can differ by orders of magnitudes, the actual simulation is preferably conducted in lattice units to avoid inaccuracies and instabilities. For coupling, the factors in the equations either have to be adjusted or the quantities temporarily converted back. This is done by the accessing the matching conversion factors in the `AdsorptionConverter`. The choice for the conversion factors for the concentration and particle density is relatively straightforward:

$$C_C = C_0, \quad C_\rho = \rho_B \,, \tag{3.35}$$

where C_0 is the inlet concentration and ρ_B is the bed density, when necessary a particle inlet concentration might be used. The conversion for the loading requires some more thought. We don't actually use the loading q but C_q, which has the units $\mathrm{g\,m^{-3}}$. There are several factors that determine the maximum occurring loading concentration C_q in a simulation, such as the isotherm, solute concentration and particle concentration. Choosing the same factor as for the particle concentration results in values that are of the same magnitude as the corresponding loading q. So, during simulation we use the conversion

$$C_{\bar{q}} = C_\rho \, C_{\bar{q}}^\star \,. \tag{3.36}$$

It is important to remember however, that, in the case of varying particle density, the actual loading that corresponds to the loading concentration is dependent on the local particle concentration

$$\bar{q}(x) = \rho_B(x) \, C_{\bar{q}}(x) \,. \tag{3.37}$$

Chapter 4
Application

The linear driving force model that was introduced in the previous sections is used in the following section in several simulations to validate its accuracy and demonstrate its practical application. Although the model is applicable without any changes to two- and three-dimensional problems, all simulations were set up in 3D, because its eventual application will be in 3D applications. All simulations were performed using the *OpenLB* [6] library.

4.1 Batch Reactor

First we look at the adsorption model itself and solve the equation on its own. It can easily be applied to a batch reactor, where an analytical solution for linear isotherms exists [16] with the dimensionless quantities as defined in sec. 3.2.1. Following the linear driving force model, the dimensionless concentration X evolves over time as

$$X(T) = \frac{1}{D_b + 1} + \frac{D_b}{D_b + 1} \exp\left(-(D_b + 1)T\right) . \tag{4.1}$$

It uses a dimensionless time T with

$$T = k_s^* \, t \, . \tag{4.2}$$

4.1.1 Simulation Setup

The batch reactor is realized as a cube with periodic boundaries on all sides. The velocity for all components is zero and we can assume perfect mixing or spatially uniform conditions. This results in a system that simply solves the differential equations for adsorption, without any fluid or particle interactions.

The process parameters and material properties that were used in the simulations are listed in table 4.1.

Table 4.1: Process parameters for batch reactor.

Parameter		Value	Unit
Isotherm parameter	K	45	L/g
Inlet concentration	C_0	1	mg/L
Adsorbent bulk density	ρ_B	0.94	kg/m^3
Adsorbent density	ρ_p	1000	kg/m^3
Column length	L	0.1	m
Particle radius	r_p	1.5×10^{-4}	m
Surface diffusion coefficient	D_s	5×10^{-11}	m^2/s^2
Film diffusion coefficient	D_f	7×10^{-11}	m^2/s^2

The model can also be made to include film diffusion. That system of equations is shown in eq. (3.6) and (3.7). There is an analytical solution for pure film diffusion as well, it is structurally the same as eq. (4.1) but with a differently defined dimensionless time T. In the case of film diffusion

$$T = \frac{k_f^*}{D_b} t \tag{4.3}$$

where, in the style of the surface diffusion coefficient, $k_f^* = \frac{3k_f}{r_p}$. As previously stated, the new boundary condition for the surface concentration has to be solved numerically.

4.1.2 Results

The evolution of the concentration in the reactor C over time can be seen in fig. 4.1. The concentration is homogenous in the entire reactor because we solve an equation that only depends on time. The top x-axis shows the dimensionless time T, the bottom axis the time t in seconds. When using the dimensionless T, the shape of the curve only depends on the value of D_b which, for a linear isotherm, is a function of the slope of the isotherm K and the bulk density of the adsorbent ρ_B alone. Specific kinetics are then introduced through the conversion to time t.

We get good agreement with the analytical solution of the linear driving force model in eq. (4.1) as shown by Worch [16]. This of course only demonstrates the correct implementation of the model and the convergence of the discretized equations towards the model equation. On the topic of the accuracy of the model itself and the validity of the model in the first place, the reader may refer to existing literature [25], [27], [31] and appendix A.

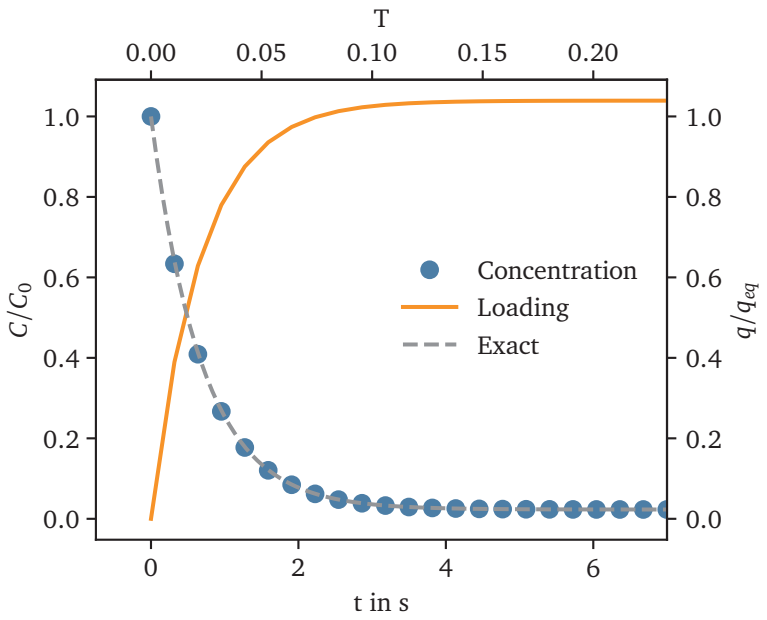

Figure 4.1: Concentration in batch reactor with surface diffusion and linear isotherm.

Fig. 4.1 also shows the amount of adsorbate taken up by the adsorbent. In the case of a batch reactor this loading curve is a mirror of the concentration. The result of the simulation is the loading concentration C_q which can be transformed to the loading by dividing through the particle density ρ_B. The equilibrium loading q_{eq} is the amount of solute adsorbed in the state of equilibrium. For the system depicted above with a linear isotherm, C_{eq} was determined through the simulation to be 0.0231 mg/L which corresponds to an equilibrium loading of 1.0393 mg/g.

Experiments with different isotherms are shown in fig. 4.2. With the kinetic (diffusion) parameters being the same, the influence of the equilibrium on the rate of the reaction is clearly visible. The same magnitude for the parameters was used (the units are different) and so the shape of the isotherms themselves and the equilibrium loading vary to a similar degree as the curve shown. Although the equilibrium concentration has not quite been reached yet after 6 seconds, it is higher for the Langmuir isotherm depicted in fig 4.2.

The LDF model was developed for surface diffusion, but film diffusion can be added as a boundary condition for the concentration. In order to test film diffusion on its own, we can use a very small Biot number Bi to eliminate the influence of surface diffusion. The results of pure film diffusion with Bi of order 1×10^{-10} are shown in fig. 4.3 together with the previous result as a comparison. We can again see good agreement with the analytical solution and conclude that the addition of film

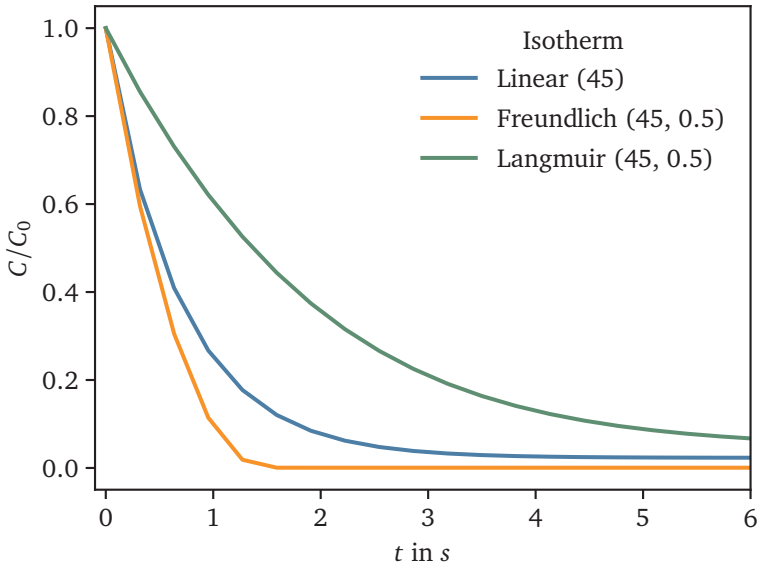

Figure 4.2: Concentration in batch reactor with different adsorption isotherms. The isotherm parameters are given in parentheses with the first one being the factor with the same unit as the loading (q_m and K).

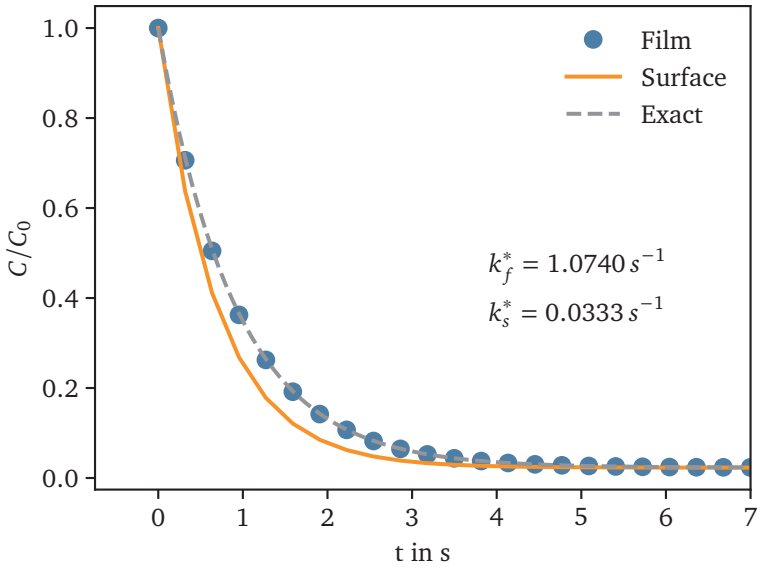

Figure 4.3: Concentration in batch reactor with film diffusion and linear isotherm.

diffusion was successful. The two mechanisms can of course be easily used in conjunction, just by setting their respective mass transfer coefficients to appropriate values.

Convergence

Because an analytical solution is known, we can very easily assess the error of the simulation. The $\mathcal{L}_2$ error of the simulation as described in eq. (3.32) and the analytical solution of (4.1) is shown in fig. 4.4 If we use diffusive scaling, which is the standard approach for LBM, we get an EOC of 2. The relaxation time τ_{ADE} is 0.6.

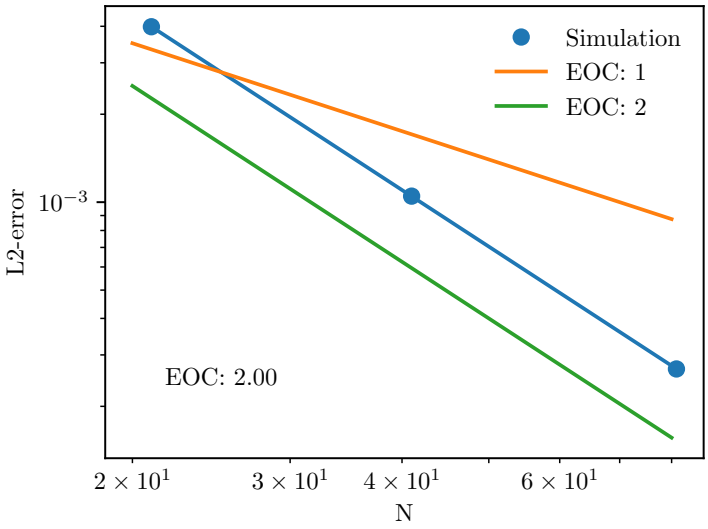

Figure 4.4: L2-error for batch reactor using diffusive scaling with the number of spatial steps on the abscissa. The simulation results for different spatial resolutions are marked with blue dots.

In this case the solution only depends on the time and because the concentration is homogenous at all time, diffusion does not play a role. So, additionally the error is plotted over the time step in fig. 4.5. Now we only achieve an EOC of 1. Diffusive scaling means $\Delta t \propto \Delta x^2$, so this finding suggests that we only have a convergence order of 1 for the time step. The previous EOC of 2 was then caused by the quadratic scaling of the time step and the actual convergence is of order one. When using acoustic scaling the EOC is always 1.

Simulations with a prescribed source term as function of time and an analytical solution as it was used by Seta [47] were conducted and show a similar convergence behavior (see appendix B). Since that test doesn't use the adsorption model at all, this suggests that this convergence behavior is not related to the particular source term proposed in this thesis.

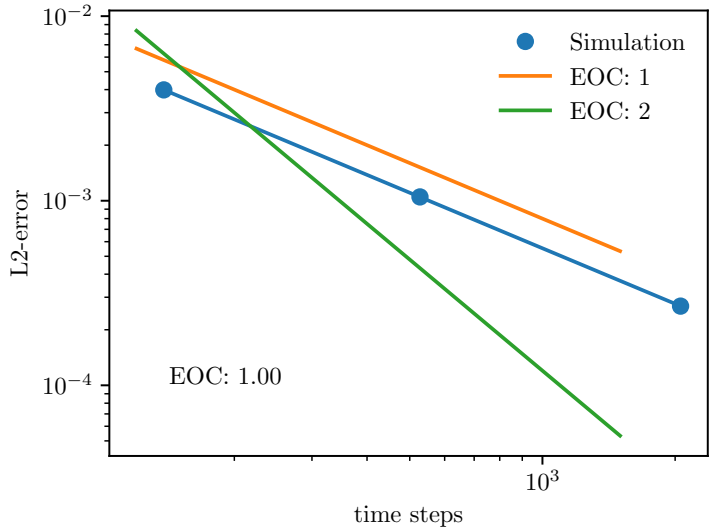

Figure 4.5: Error for batch reactor using acoustic scaling with the number of time steps on the abscissa. The simulation results for different time steps are marked with blue dots.

4.2 Fixed Bed Reactor

After having validated the solution to the equations describing mass transfer of adsorption, the next step is to look at a fixed bed reactor with moving solute. The goal here is to validate the combination of the advection diffusion equation with the source term from adsorption.

Once an equilibrium has been reached and the constant pattern behavior is established, the analytical solution found by [23] for both the Langmuir and Freundlich isotherm applies. Adapted to non-dimensional values [16] we get an implicit equation for the concentration X with

$$\frac{R}{1-R}\log(X) - \frac{1}{1-R}\log(1-X) = N_s(-T+1) + \delta_I \tag{4.4}$$

where the dimensionless quantities T, X and N_s are used, with

$$T = \frac{t}{t_{\text{st}}}, \quad X = \frac{c}{C_0} \quad \text{and} \quad N_s = k_s^* t_{\text{st}} \tag{4.5}$$

and an integration constant δ_I. We assume that the residence time t_r can be neglected. The separation factor R for the Langmuir isotherm is

$$R = \frac{1}{1 + b\,C_0}\,. \tag{4.6}$$

This is the solution to a plug-flow model, meaning dispersion (e.g. diffusion) is not accounted for. Our model used for the simulation is a dispersed-flow model because it includes a diffusion term.

4.2.1 Method

Eq. (4.4) is implicit, so we need to solve it numerically for use in the error calculations. This was done using *scipy's fsolve* function, which uses a modified Powell method. The integration constant δ_I can be found using the material balance of a BTC:

$$\int_{T=0}^{T(X=1)} (1 - X)\ dT = 1\,. \tag{4.7}$$

Some exemplary values can be found in [16].

Once the constant pattern has been reached, the eventual breakthrough curve has already formed inside the column as the concentration front. We can transform the x-axis to convert between the two. Time and length along the column can be converted by mirroring around x_{st} using $t = 2x_{st} - x$ and because we use the dimensionless time $T = t/t_{st}$ with $t = \frac{q_{0,eq}\,A\,x}{C_0\dot{V}}$, all factors cancel each other. In combination and additionally centering around $T = 1$ we get

$$T = \frac{t}{t_{st}} = \frac{2x_{st} - x}{x_{st}}\,, \tag{4.8}$$

where x_{st} is the position of the center of mass of the BTC, approximated as the position x where $C/C_0 = 0.6$. This procedure removes any influence of the outlet boundary on the shape of the breakthrough curve because we sample from the center of the column.

4.2.2 Simulation Setup

The reactor is realized as a three-dimensional cuboid with periodic boundary conditions on all sides except the inlet and outlet. A constant fluid velocity is set for the entire volume. The inlet has a Dirichlet boundary condition with C_0. The process parameters are listed in table 4.2. While the adsorbent bulk density may be uncharacteristically low for a fixed bed reactor, it is reasonable for a slurry reactor and reduces the simulation time considerably. The reason is twofold: first, the stoichiometric time t_{st} is proportional to the mass of adsorbent, so more adsorbent

Table 4.2: Process parameters for fixed bed reactor.

Parameter		Value	Unit
Isotherm parameter 1	q_m	20	mg/g
Isotherm parameter 2	b	0.8	mg/g
Inlet concentration	C_0	1	mg/L
Adsorbent bulk density	ρ_B	1	kg/m^3
Column length	L	0.05	m
Column width	a	0.0016	m
Particle radius	r_p	3×10^{-4}	m
Surface diffusion coefficient	D_s	5×10^{-11}	m^2/s^2

means later breakthrough, and secondly, the increased mass of adsorbent leads to larger reaction rates, which has implications for stability. To counteract this, the time steps have to be increased, which leads to a longer simulation time.

4.2.3 Results

Fig. 4.6 shows the concentration profile in the column after 3400 seconds. The stoichiometric time t_{st} in this case is about 6800 seconds, which leads to the MTZ being roughly centered and enables a clean plot. The intraparticle mass transfer rate $N_s = 28$ is adjusted to reflect that the breakthrough curve was taken at the midpoint of the column. Had the full length of the column been used, the value would be 56.

The breakthrough curve that resulted from the transformation previously mentioned is shown in fig 4.7. It shows good agreement with the analytical solution. There are no obvious deviations in the shape of the curve. We see the characteristic shape of a breakthrough curve with dominating surface diffusion: the curve is not symmetrical around $T = 1$, instead it is slightly flatter for larger concentrations.

Two ways to align the measured curves and the solution are possible. The first is to calculate the expected position of the center of mass and shift the curve by that value, the second is to try and find the center of mass of the actual measured curve. For symmetrical curves this point is $0.5\,C_0$. Because in this case surface diffusion dominates, it is actually around $0.56\,C_0$. In this section all plots are aligned using the second method, so that they all cross exactly at $T = 1$, and we can concentrate on the differences in shape. We will discuss the alignment error separately.

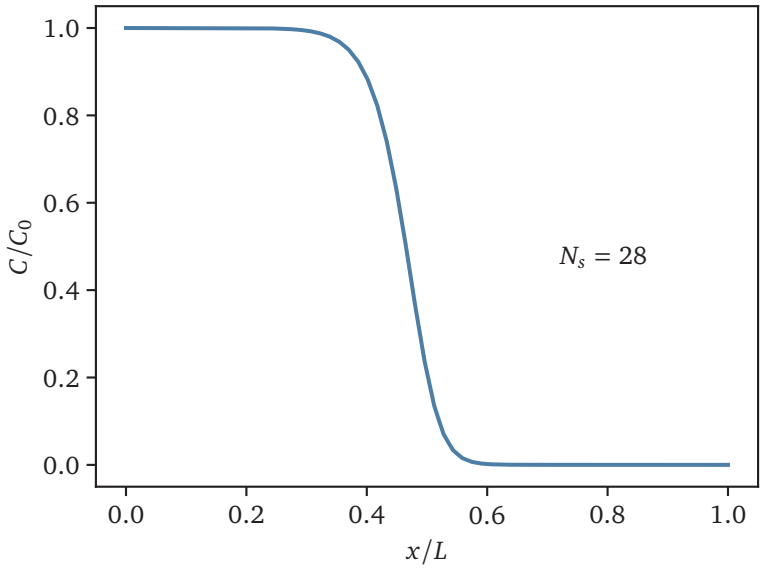

Figure 4.6: Concentration profile for fixed bed reactor with N=21 at t = 3400s.

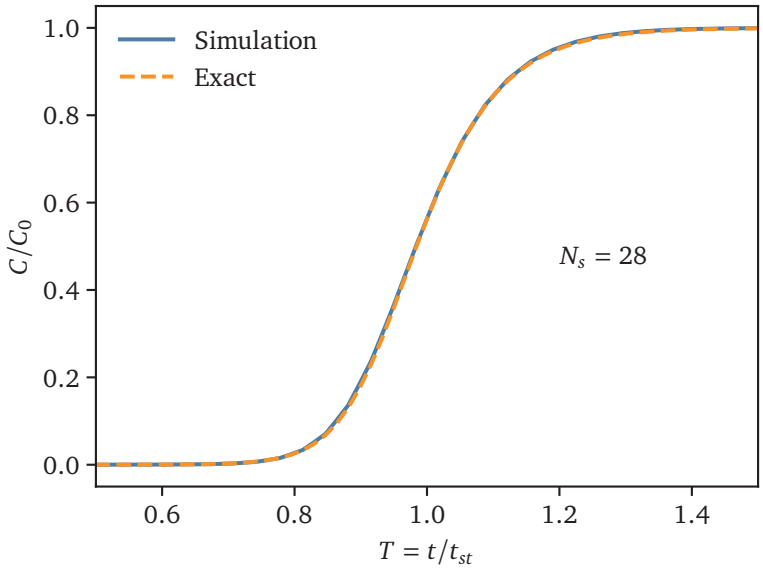

Figure 4.7: Breakthrough curve for fixed bed reactor with N=21.

The expected position of the MTZ at any point in time can be calculated by rearranging eq. (2.27) to get the column position $h(t)$. For t we insert the simulation time t_{sim}. If we compare the expected position and our approximation from the measured curve we get a relative error of around 2%.

The influence of the kinetics and isotherm on the shape can be seen in fig. 4.8. The surface diffusion mass transfer parameter k_s^* is proportional to D_s and determines

the speed of the mass transfer. For larger values, which is shown by the green curve in fig. 4.8, the curve comes closer to the ideal breakthrough curve with a vertical concentration front. All the curves in fig. 4.8 show a Langmuir isotherm, where a

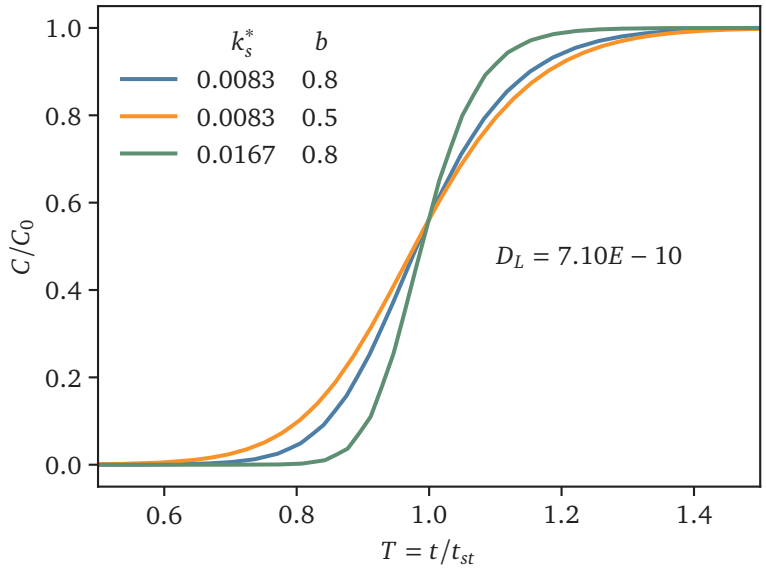

Figure 4.8: Breakthrough curve in fixed bed reactor with different kinetic and isotherm parameters.

larger parameter b results in a steeper isotherm. As expected, the orange curve with $b = 0.5$ is indeed flatter.

Our implementation allows easy access to the value of the source term at any point in time. This is depicted in fig. 4.9 for two separation factors R. A smaller value for R can be caused by a steeper isotherm or a larger initial concentration. The source term is shown as a dotted line. It is clearly visible that the peak's height as well as the shape of the curve are different. For larger R the curve is more asymmetrical with a steeper rise and a longer tail, which is typical for surface diffusion control. This is also visible in the breakthrough curve.

The solution given in eq. (4.4) does not include diffusion. This however is impossible to replicate with the approach used in this thesis, since we solve the advection diffusion equation. The influence of diffusion can be seen in fig. 4.10. For larger values of D the curve flattens and the breakthrough point appears earlier. We can see that for values of $D = 5 \times 10^{-11}$, which corresponds to $Sc = 1559$, we already get very good agreement with the analytical solution. Although in this example the particles are fixed in place, and therefore the advection part of eq. (2.37) is irrelevant, diffusion does play a large role. The diffusion coefficient of the particle

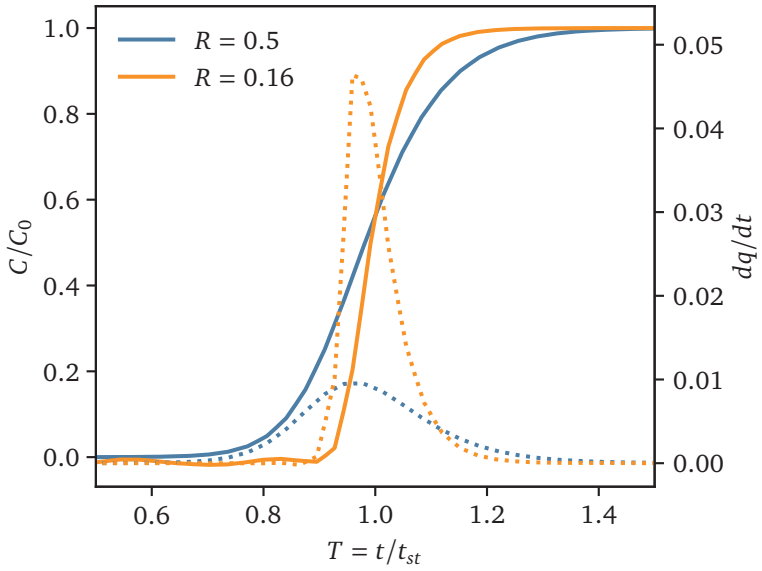

Figure 4.9: Concentration and source term for different separation factors.

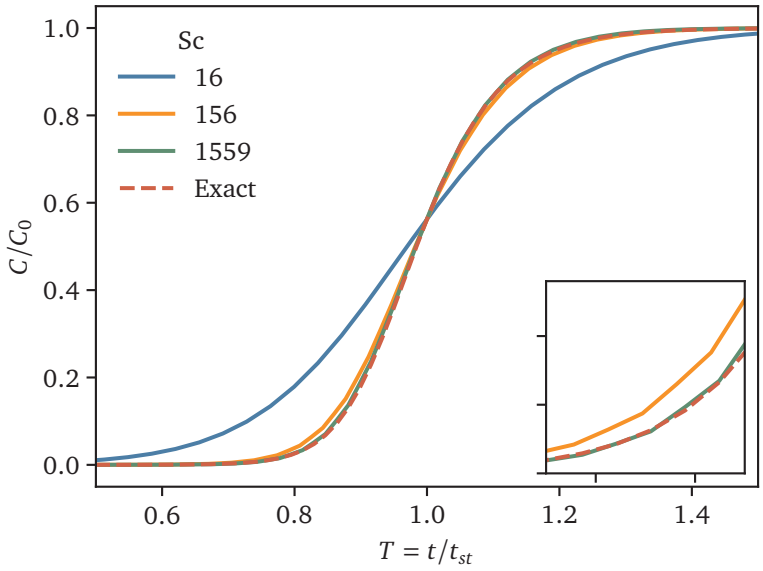

Figure 4.10: Breakthrough curve for different diffusion coefficients with N=21.

and loading lattices also have an impact on the result. Since we are investigating the convergence to $D \to 0$ and not any specific substance, all ADE lattices used the same diffusion coefficient.

Convergence

A series of simulations with a fixed diffusion coefficient will not converge to the analytic solution, for this reason Δx, Δt and Sc are scaled together. When scaling in a ratio of 1:1:1, this will keep the relaxation parameter τ constant, similar to diffusive scaling. In this case $\tau_{\text{ADV}} = 0.501$. The resulting errors are shown in fig. 4.11. It

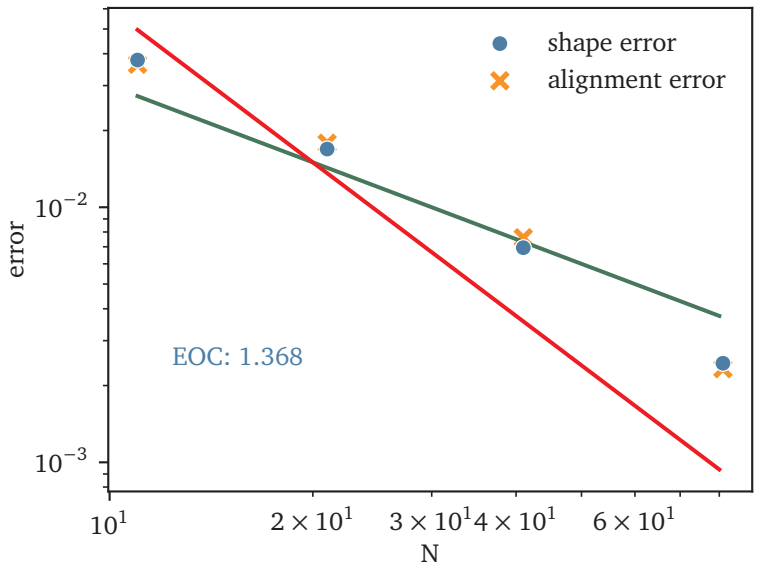

Figure 4.11: Error based on shape and position along the column for different resolutions N.

shows both the error caused by differing shapes and the difference in the position of the center of mass of the curve, called alignment error. Surprisingly they both have very similar values as well as convergence behavior. The order of convergence is around 1.37. This means that we get convergence towards a non-dispersive solution even when using a dispersed-flow model.

Just looking at the fluid diffusion, it contributes an error around order 0.75. Interestingly the alignment error increases with increasing Sc. This can be seen in fig. 4.12, which shows the convergence purely based on diffusion with no changes in Δx or Δt, instead with changing relaxation parameters τ_{ADV} ranging from 0.52 to 0.5002.

Fixed bed reactors can be modelled very well by the linear driving force model [25] and we have now demonstrated that our model does so as well.

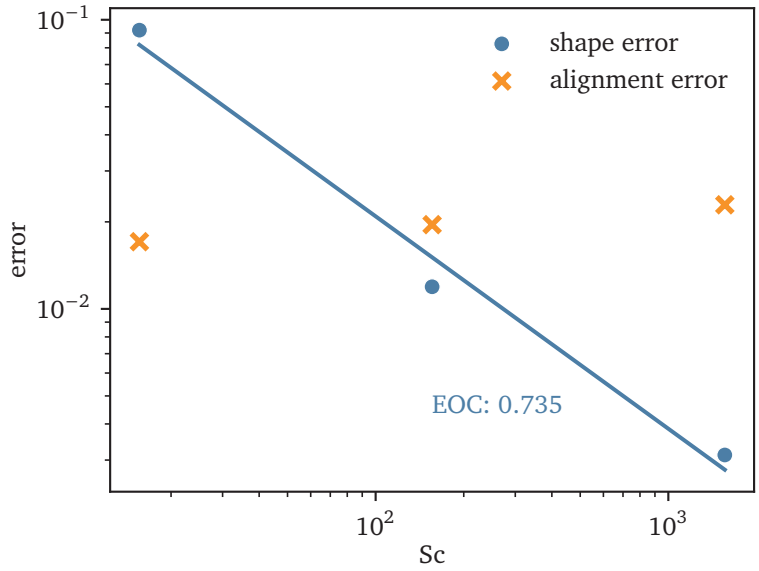

Figure 4.12: Error based on shape and position along the column for different Sc and fixed resolution.

Volume Averaged Equations

As a step towards its future use the simulations were also performed using the volume averaged Navier Stokes equations. By taking the porosity into account the volume that is available for the fluid decreases and so the flow rate of solute decreases as well. This will lead to longer stoichiometric times. In the adsorption model this is accounted for only in a porosity factor in the source term for the solute concentration. Because we divide by the stoichiometric time t_{st}, a correct implementation of the VANS equations has therefore no effect on the results in the nondimensionalised graph.

Fig. 4.13 shows the concentration profiles for two simulations, one with the NSE and one with the VANSE. The center of mass of the curves x_c is marked with dashed lines. The shape is again caused by the smaller value of the intraparticle mass transfer rate N_s used in these simulations and is to be expected. The breakthrough time is proportional to the porosity ϵ and the position of the center of mass x_c is inversely proportional.

Table 4.3 shows the breakthrough times and curve positions for two different porosities and their ratios. The numerator and denominator in the ratios for the time and distance are chosen so that in each case they reflect the porosity. Porosity of 1 in this context means that porosity is not taken into account. The two simulations

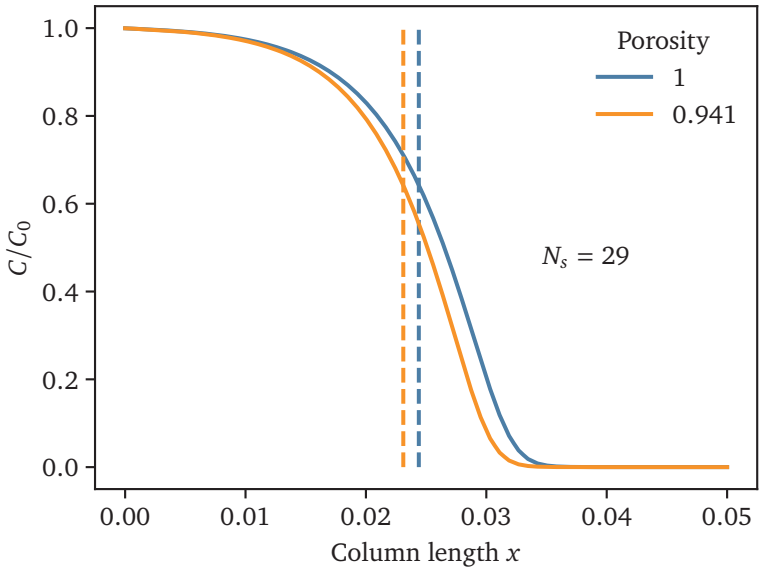

Figure 4.13: Concentration profile for different porosities. The vertical lines mark the center of mass of the curve.

have a ratio of 0.9471, which matches the porosity with a relative error of 0.0063 or about 0.63%. This was achieved with a resolution of 21 nodes and $\tau_{\text{ADE}} = 0.5001$.

Table 4.3: Breakthrough curve parameters and corresponding ratios

Quantity	NSE	VANS	Ratio
ε	1	0.941	0.941
t_{st} (s)	6410	6810	0.941
x_{st} (m)	0.0244	0.0229	0.941
x_c (m)	0.0244	0.0231	0.9471

Table 4.4: Process parameters for porosity investigations in a fixed bed reactor

Parameter		Value	Unit
Isotherm parameter 1	q_m	1	mg/g
Isotherm parameter 2	b	0.5	mg/L
Inlet concentration	C_0	10	mg/L
Adsorbent bulk density	ρ_B	100	kg/m^3
Particle radius	r_p	5×10^{-4}	m

As the parameters of the two most recent simulations are in some places quite different, the new values are listed in table 4.4.

4.3 Static Mixer

As an example for a more industrial application a static mixer was chosen. This showcases all aspects of the model with moving solute and fluid and moving particles, which means a variable particle density. While the linear driving model is especially suitable for a fixed bed reactor, with the modifications proposed in this thesis, it can also be applied to other scenarios like this. For this much more complicated setup there was no solution or experimental results available for comparison, but it can be used as a more illustrative example of the possibilities of the model.

4.3.1 Simulation Setup

The geometry of the mixer can be seen in fig 4.14 with the concentration of particles and solute after a steady state has been reached. The two other components, fluid and particle loading, are not visible. The particle loading follows the path of the particles exactly. It is zero at the inlet and only increased through adsorption after contact with the solute. Particles are injected on the left-hand side and the solute on the right side. At the upper outlet a velocity boundary is set with a velocity so

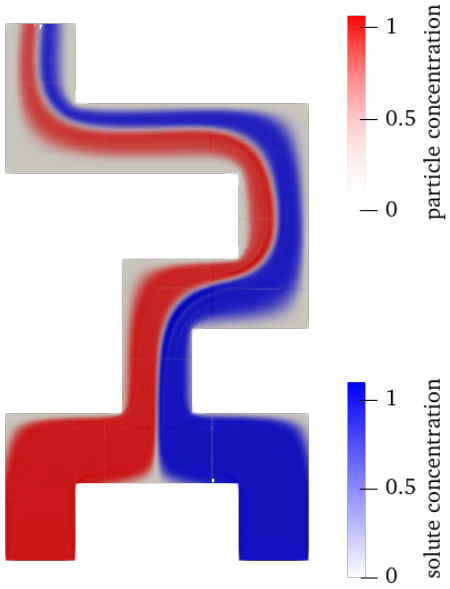

Figure 4.14: Static mixer with separate inlets for particles and solute.

that the fluid flows out at the top. The fluid velocity is one-way coupled with the other lattices, in effect dragging the solute and particles with it.

Table 4.5: Process and simulation parameters for static mixer.

Parameter	Value	Unit
q_m	20	mg/g
b	0.5	mg/L
C_0	1	mg/L
ρ_B	1	kg/m^3
L	0.0133	m
r_p	5×10^{-5}	m
D_s	5×10^{-11}	m^2/s^2
k_f	1.37×10^{-2}	m^2/s^2
τ	0.6125	

In this setup the choice of simulation parameters is restricted by the coupling demands and stability concerns brought up in sec. 3.3.4. We need the time step of all lattices to match, which can only be achieved by carefully selecting the relaxation parameters and diffusion coefficients.

4.3.2 Results

The resulting particle loading can be seen in fig 4.15. It shows a gradual mixing

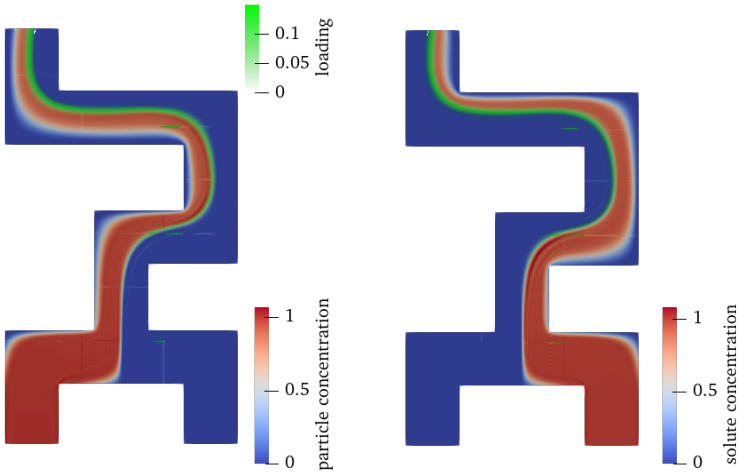

Figure 4.15: Loading (green) in a static mixer.

of the two phases and the resulting reaction product. This image shows a steady state, so all particles will experience the loading shown in the image. Because the setup has laminar flow, the mixing is relative low and particles do not experience fast changing conditions.

With a setup like this, the limits of the linear driving force model need to be kept in mind. This was described in section 2.1.3. A cyclical absorption and desorption that would occur if particles moved in and out of areas of high solute concentration might not be captured accurately. In this laminar case this inaccuracy should not be very large, because the particles and solute are coupled to the fluid and move the same way.

The advection diffusion lattices can produce negative concentrations at concentration fronts where gradients are large. This applies to both the particle and solute lattice and also occurs when there is no reaction. This can be seen in the detail view of fig. 4.16. Additionally, a wave pattern of fluctuating sign in the concentration can

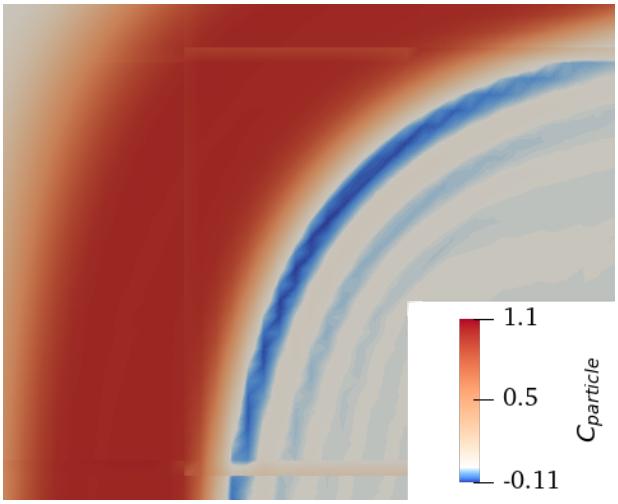

Figure 4.16: Particle concentration in mixer showing negative concentration. White represents a concentration of 0.

be seen, which originates at the concentration front. The solute concentration in fig.4.15 also shows these waves. This behavior was also observed in the fixed bed reactor but to a much smaller extent. It unfortunately also leads to negative loading, as the three lattices are directly coupled.

In conclusion, we can say that the adsorption model can be successfully applied to moving particle systems, but it is affected by stability problems of the advection diffusion solution.

Chapter 5
Conclusion

A model for adsorption on moving particles using a linear driving force was developed and incorporated into the advection diffusion reaction equation. The model can be solved using the lattice Boltzmann method with separate lattices for fluid, solute, particles and particle loading. The primary mass transport mechanism describing adsorption is surface diffusion but both external mass transfer in the form of film diffusion and alternative internal transfer mechanisms, namely pore diffusion, can be added as well. Different isotherms are possible as well.

Comparison with an analytic solution for the adsorption kinetics in a batch reactor has shown good accuracy. A convergence study showed an order of convergence of 1 for the time step and an EOC of 2 for diffusive scaling. This behavior can also be observed for other source terms that only depend on time. The model predicts breakthrough curves in a fixed bed reactor well and convergence towards the exact solution was demonstrated. The influence of different adsorption parameters and dispersion caused by diffusion was explored as well. When reducing the fluid diffusion coefficient together with the discretization steps Δx and Δt an experimental order of convergence of around 1.4 towards a no-dispersive solution can be observed.

Additionally, the volume averaged Navier Stokes equations were used to better account for the particle volume. The expected delay of the breakthrough was observed.

The model was then applied to a more complex flow in a static mixer with moving particles to demonstrate its potential for use in investigations of the influence of fluid flow on adsorption performance.

Further work can be done to implement the more accurate LDF model with variable mass transfer coefficients, if the added accuracy is needed. Desorption as seen in a moving bed reactor for example could be another area of study on the way to a complete model of adsorption processes in complex fluid flows. Difficulties with stability caused by, for example, the coupling of the ADE and NSE lattices and large source terms could be addressed by using alternative approaches like the multiple relaxation time LBM.

List of Symbols

$\bar{q}$	Average particle loading in core.
$\boldsymbol{F}$	Body force
$\boldsymbol{u}$	fluid velocity
$\dot{m}_f$	Mass flow in film diffusion
$\dot{m}_S$	Mass flow in surface diffusion
Bi	Biot number
Pe	Péclet number
Re	Reynolds number
Sc	Schmidt number
Sh	Sherwood number
Ω_i	Collision operator
ρ	density
ρ_B	Bed density / Particle concentration
ρ_P	Particle material density
A_s	Particle surface area
b	Isotherm parameter 2 for Langmuir isotherm
C	Concentration
C_0	Inlet concentration
c_i	Lattice velocity
C_s	Surface concentration
c_s	Speed of sound
D_b	Distribution factor for batch reactor

D_L Diffusion coefficient in fluid

D_s Surface diffusion coefficient

f_i Particle distribution density function

K Isotherm parameter 1

k_f^* Film diffusion mass transfer coefficient

k_s^* Surface diffusion mass transfer coefficient

m_A Adsorbent mass

m_a Mass of adsorbed substance

m_S Mass of solute

n Isotherm exponent

N_s Dimensionless mass transfer coefficient (surface diffusion)

p Pressure

q Particle loading

q_m Isotherm parameter 1 for Langmuir isotherm

$q_{0,\mathrm{eq}}$ Equilibrium loading corresponding to C_0

q_{eq} Equilibrium loading

R Separation factor

s Source term

S_i Lattice Boltzmann source term

T Dimensionless time

V_L Liquid volume

w_i Lattice Boltzmann velocity weights

X Dimensionless concentration

Y Dimensionless loading

Comparison of LDF and HSDM models

Appendix A

The homogeneous surface diffusion model (HSDM) and the linear driving force model LDF both make similar assumptions. They both only solve for surface diffusion, but the linear driving force model simplifies the concentration profile inside the particle.

For both models an analytical solution exists when using a linear isotherm. The solution for the LDF was shown in (4.1), the solution for the HSDM [53] is

$$X = 1 - \frac{1}{1 + D_B}\left(1 - \sum_{n=1}^{\infty} \frac{6D_B(D_B + 1)\exp(-u_n^2 T_B)}{9 + 9D_B + u_n^2 D_B^2}\right), \tag{A.1}$$

where u_n is the nth root of

$$\tan u_n = \frac{3u_n}{3 + D_B u_n^2}. \tag{A.2}$$

An example solution for both models can be seen in fig. A.1. While the LDF clearly differs from the more accurate HSDM solution, it does capture the shape of the curve reasonably well, while being much easier to solve[16], [54].

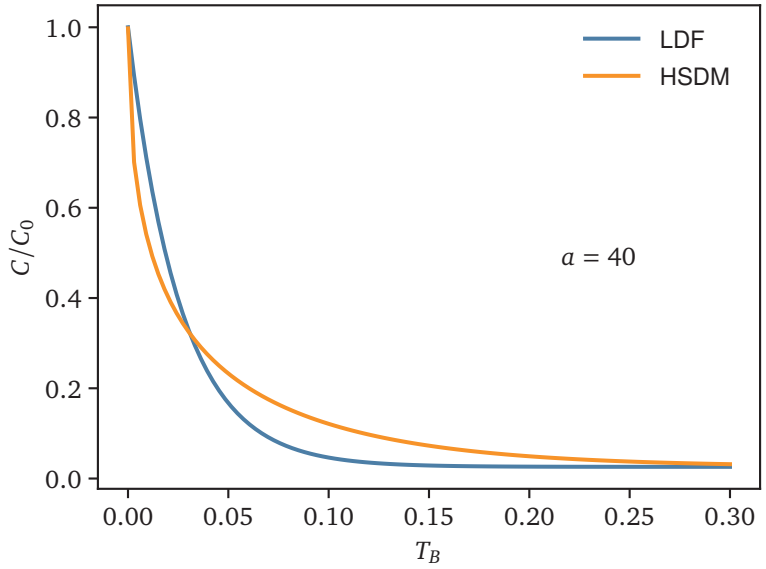

Figure A.1: Comparison of HSDM and LDF kinetic models.

Source Term Validation

Appendix B

We want to, first and foremost, determine the temporal convergence of a source term, because the adsorption source term only depends on time. Following the example in Seta [47] a time dependent source term given by a function is imposed. The equation to be solved is

$$\frac{\partial T}{\partial t} + \boldsymbol{u} \cdot T = D\nabla^2 T + Q\,. \tag{B.1}$$

Prescribing the source term to be only a function of time, later called type *exp*,

$$Q = \alpha \exp(\alpha t) \tag{B.2}$$

results in the solution

$$T(x, y) = \exp(\alpha t)\,. \tag{B.3}$$

The velocity is zero, so no contribution of the advection term is expected.

The relative L_2 error is shown in fig. B.1 marked as blue. It exhibits an order of convergence of 1 for both acoustic and diffusive scaling.

On the other hand, prescribing the source term with a spatial component (type *sin*) to be

$$Q = \left(\alpha + 2D\kappa^2\right) \sin(\kappa x) \sin(\kappa y) \exp(\alpha t) \tag{B.4}$$

results in the solution

$$T(x, y) = \sin(\kappa x) \sin(\kappa y) \exp(\alpha t)\,. \tag{B.5}$$

The results, together with the previous, can be seen in fig. B.1. With these four sets of errors we can try to figure out the different contributions of spatial and temporal scaling. As we saw before, when the source is only a function of time, the convergence with respect to time is one. When the solution contains a space dependent term, there is a difference between the scaling methods. In the spatially varying case acoustic scaling actually produces a better EOC. This can be explained by the fact that in the first case (B.2) the spatial resolution has no effect on the error,

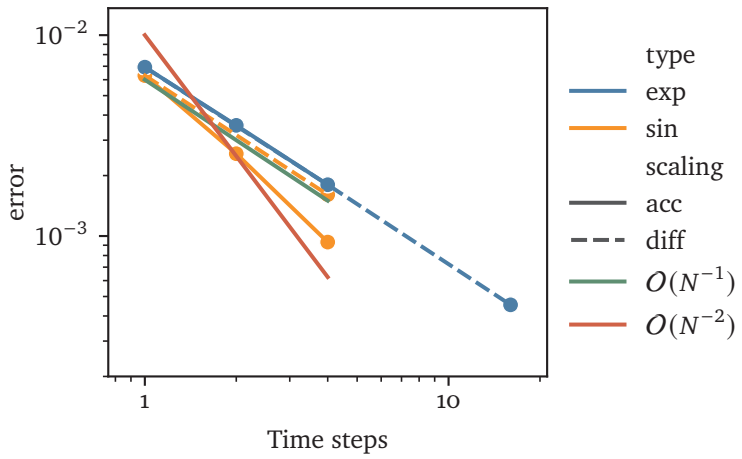

Figure B.1: Temporal convergence of analytical source term.

whereas in the second case (B.4) it does and the spatial convergence is better than the temporal.

If we now plot the error over the spatial grid number N in fig. B.2, we see again a worse EOC for acoustic scaling. For diffusive scaling we see a much better EOC for the exponential function, however we have to keep in mind, that that is more a function of having scaled $\Delta t \sim \Delta x^2$ than anything else. The actual convergence is close to one, since the reduction in Δx does not actually decrease the error in this case. For (B.4) we see an EOC of 2 for diffusive scaling, which is the optimal

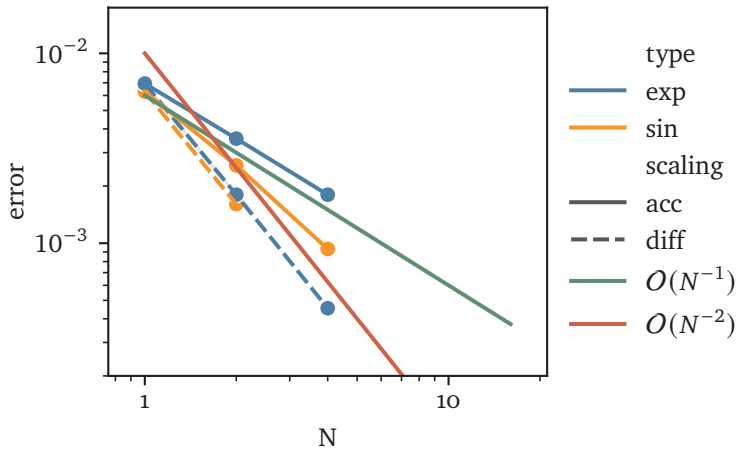

Figure B.2: Spatial convergence of analytical source term.

outcome and can be explained by the fact that in this case both the decreasing of Δt and Δx contribute to the reduction of the error.

Bibliography

[1] A. Dąbrowski, "Adsorption — from theory to practice," *Advances in Colloid and Interface Science*, vol. 93, no. 1-3, pp. 135–224, 2001, ISSN: 0001-8686. DOI: 10.1016/S0001-8686(00)00082-8. [Online]. Available: https://www.sciencedirect.com/science/article/pii/S0001868600000828.

[2] U. Berg, G. Knoll, E. Kaschka, *et al.*, "P-roc-phosphorus recovery from wastewater by crystallisation of calcium phosphate compounds," *Journal of residuals science and technology*, vol. 4, no. 3, 2005. [Online]. Available: https://pap.co.at/fileadmin/user_upload/publications/2005_Phosphorus_Recovery_Johannesburg.pdf.

[3] D. C. S. de Azevedo, "Separation/reaction in simulated moving bed application to the production of industrial sugars," Ph.D. dissertation, University of Porto, Porto, 2001.

[4] T. Henn, G. Thäter, W. Dörfler, H. Nirschl, and M. J. Krause, "Parallel dilute particulate flow simulations in the human nasal cavity," *Computers & Fluids*, vol. 124, pp. 197–207, 2016, ISSN: 00457930. DOI: 10.1016/j.compfluid.2015.08.002.

[5] T. Krüger, H. Kusumaatmaja, A. Kuzmin, O. Shardt, G. Silva, and E. M. Viggen, *The Lattice Boltzmann Method*. Cham: Springer International Publishing, 2017, ISBN: 978-3-319-44647-9. DOI: 10.1007/978-3-319-44649-3.

[6] M. J. Krause, A. Kummerländer, S. J. Avis, *et al.*, "Openlb—open source lattice boltzmann code," *Computers & Mathematics with Applications*, vol. 81, pp. 258–288, 2021, ISSN: 0898-1221. DOI: 10.1016/J.CAMWA.2020.04.033.

[7] G. Long, X. Lizhi, S. Xiaowen, and Z. Xiaoling, "Modeling adsorption with lattice boltzmann equation," *Scientific Reports 2016 6:1*, vol. 6, no. 1, pp. 1–9, 2016, ISSN: 2045-2322. DOI: 10.1038/srep27134. [Online]. Available: https://www.nature.com/articles/srep27134.

[8] S. Agarwal, N. Verma, and D. Mewes, "A lattice boltzmann model for adsorption breakthrough," *Heat and Mass Transfer 2005 41:9*, vol. 41, no. 9, pp. 843–854, 2005, ISSN: 1432-1181. DOI: 10.1007/S00231-005-0625-X. [Online]. Available: https://link.springer.com/article/10.1007/s00231-005-0625-x.

[9] N. Manjhi, N. Verma, K. Salem, and D. Mewes, "Lattice boltzmann modelling of unsteady-state 2d concentration profiles in adsorption bed," *Chemical Engineering Science*, vol. 61, no. 8, pp. 2510–2521, 2006, ISSN: 00092509. DOI: 10.1016/j.ces.2005.11.018.

[10] Z. Peng, S. Liu, Y. Li, Z. Deng, and H. Feng, "Pore-scale lattice boltzmann simulation of gas diffusion–adsorption kinetics considering adsorption-induced diffusivity change," *Energies*, vol. 13, no. 18, p. 4927, 2020. DOI: 10.3390/en13184927. [Online]. Available: https://www.mdpi.com/1996-1073/13/18/4927.

[11] Z. Peng, Z. Deng, H. Feng, S. Liu, and Y. Li, "Multiscale lattice boltzmann simulation of the kinetics process of methane desorption-diffusion in coal," *ACS Omega*, vol. 6, no. 30, pp. 19 789–19 798, 2021. DOI: 10.1021/acsomega.1c02499.

[12] M.-L. Maier, S. Milles, S. Schuhmann, G. Guthausen, H. Nirschl, and M. J. Krause, "Fluid flow simulations verified by measurements to investigate adsorption processes in a static mixer," *Computers & Mathematics with Applications*, vol. 76, no. 11-12, pp. 2744–2757, 2018, ISSN: 0898-1221. DOI: 10.1016/j.camwa.2018.08.066.

[13] Q. Ma, Z. Chen, and H. Liu, "Multiple-relaxation-time lattice boltzmann simulation for flow, mass transfer, and adsorption in porous media," *Physical review. E*, vol. 96, no. 1-1, p. 013 313, 2017. DOI: 10.1103/PhysRevE.96.013313.

[14] D. Micale, R. Uglietti, M. Bracconi, and M. Maestri, "Coupling euler-euler and microkinetic modeling for the simulation of fluidized bed reactors: An application to the oxidative coupling of methane," *Industrial & Engineering Chemistry Research*, vol. 60, no. 18, pp. 6687–6697, 2021, ISSN: 0888-5885. DOI: 10.1021/acs.iecr.0c05845.

[15] L. A. Vandewalle, G. B. Marin, and K. M. van Geem, "Catchyfoam: Euler–euler cfd simulations of fluidized bed reactors with microkinetic modeling of gas-phase and catalytic surface chemistry," *Energy & Fuels*, vol. 35, no. 3, pp. 2545–2561, 2021, ISSN: 0887-0624. DOI: 10.1021/acs.energyfuels.0c02824.

[16] E. Worch, *Adsorption technology in water treatment: Fundamentals, processes, and modeling*, 2nd, revised edition. Berlin Germany and Boston: De Gruyter, 2021, ISBN: 9783110715422.

[17] K. Y. Foo and B. H. Hameed, "Insights into the modeling of adsorption isotherm systems," *Chemical Engineering Journal*, vol. 156, no. 1, pp. 2–10, 2010, ISSN: 1385-8947. DOI: 10.1016/j.cej.2009.09.013. [Online]. Available: https://www.sciencedirect.com/science/article/pii/S1385894709006147.

[18] D. M. LeVan, G. Carta, and K. S. Walton, "Adsorption and ion exchange," in *Perry's chemical engineers' handbook*, D. W. Green and M. Z. Southard, Eds., New York: McGraw Hill Education, 2019, pp. 16-1 - 16–54, ISBN: 9780071834094.

[19] M. Islam, M. Khan, and M. Mozumder, "Adsorption equilibrium and adsorption kinetics: A unified approach," *Chemical Engineering & Technology*, vol. 27, no. 10, pp. 1095–1098, 2004, ISSN: 0930-7516. DOI: 10.1002/ceat.200402084.

[20] J. Wang and X. Guo, "Adsorption kinetic models: Physical meanings, applications, and solving methods," *Journal of Hazardous Materials*, vol. 390, p. 122156, 2020, ISSN: 0304-3894. DOI: 10.1016/j.jhazmat.2020.122156. [Online]. Available: https://www.sciencedirect.com/science/article/pii/S0304389420301448.

[21] X. He, N. Li, and B. Goldstein, "Lattice boltzmann simulation of diffusion-convection systems with surface chemical reaction," *Molecular Simulation*, vol. 25, no. 3-4, pp. 145–156, 2000, ISSN: 0892-7022. DOI: 10.1080/08927020008044120. [Online]. Available: https://www.tandfonline.com/doi/pdf/10.1080/08927020008044120?needAccess=true (visited on 10/31/2021).

[22] G. L. Dotto, N. P. G. Salau, J. S. Piccin, T. R. S. Cadaval, and L. A. A. de Pinto, "Adsorption kinetics in liquid phase: Modeling for discontinuous and continuous systems," in *Adsorption Processes for Water Treatment and Purification*, A. Bonilla-Petriciolet, D. I. Mendoza Castillo, and H. E. Reynel-Ávila, Eds., Cham: Springer, 2017, pp. 53–76, ISBN: 978-3-319-58136-1. DOI: 10.1007/978-3-319-58136-1_3.

[23] E. Glueckauf and J. I. Coates, "Theory of chromatography; the influence of incomplete equilibrium on the front boundary of chromatograms and on the effectiveness of separation," *Journal of the Chemical Society (Resumed)*, no. 0, pp. 1315–1321, 1947, ISSN: 0368-1769. DOI: 10.1039/JR9470001315. [Online]. Available: https://pubs.rsc.org/en/content/articlelanding/1947/jr/jr9470001315/unauth.

[24] H.-K. Hsuen, "An improved linear driving force approximation for intraparticle adsorption," *Chemical Engineering Science*, vol. 55, no. 17, pp. 3475–3480, 2000, ISSN: 00092509. DOI: 10.1016/S0009-2509(99)00600-4. [Online]. Available: https://www.sciencedirect.com/science/article/pii/S0009250999006004.

[25] S. Sircar and J. R. Hufton, "Why does the linear driving force model for adsorption kinetics work?" *Adsorption*, vol. 6, no. 2, pp. 137–147, 2000, ISSN: 1572-8757. DOI: 10.1023/A:1008965317983. [Online]. Available: https://link.springer.com/article/10.1023/A:1008965317983.

[26] C. H. Liaw, J. S. P. Wang, R. A. Greenkorn, and K. C. Chao, "Kinetics of fixed-bed adsorption: A new solution," *AIChE Journal*, vol. 25, no. 2, pp. 376–381, 1979, ISSN: 1547-5905. DOI: 10.1002/aic.690250229. [Online]. Available: https://aiche.onlinelibrary.wiley.com/doi/10.1002/aic.690250229.

[27] K. Hashimoto and K. Miura, "A simplified method to design fixed-bed adsorbers for the freundlich isotherm," *JOURNAL OF CHEMICAL ENGINEERING OF JAPAN*, vol. 9, no. 5, pp. 388–392, 1976, ISSN: 0021-9592. DOI: 10.1252/jcej.9.388. [Online]. Available: https://www.jstage.jst.go.jp/article/jcej1968/9/5/9_5_388/_article.

[28] E. Worch, "Fixed-bed adsorption in drinking water treatment: A critical review on models and parameter estimation," *Journal of Water Supply: Research and Technology-Aqua*, vol. 57, no. 3, pp. 171–183, 2008, ISSN: 0003-7214. DOI: 10.2166/aqua.2008.100.

[29] I. Neretnieks, "Analysis of some adsorption experiments with activated carbon," *Chemical Engineering Science*, vol. 31, no. 11, pp. 1029–1035, 1976, ISSN: 00092509. DOI: 10.1016/0009-2509(76)87023-6. [Online]. Available: https://www.sciencedirect.com/science/article/pii/0009250976870236.

[30] D. M. Ruthven, *Principles of adsorption and adsorption processes*. New York and Chichester: Wiley, 1984, ISBN: 0471866067.

[31] T. Choong and D. M. Scott, "The linear driving force model for cyclic adsorption and desorption: The effect of external fluid-film mass transfer," *Chemical Engineering Science*, vol. 53, no. 4, pp. 847–851, 1998, ISSN: 00092509. DOI: 10.1016/S0009-2509(97)00345-X. [Online]. Available: https://www.sciencedirect.com/science/article/pii/S000925099700345X.

[32] S.-I. Nakao and M. Suzuki, "Mass transfer coefficient in cyclic adsorption and desorption," *JOURNAL OF CHEMICAL ENGINEERING OF JAPAN*, vol. 16, no. 2, pp. 114–119, 1983, ISSN: 0021-9592. DOI: 10.1252/jcej.16.114. [Online]. Available: https://www.jstage.jst.go.jp/article/jcej1968/16/2/16_2_114/_article/-char/ja/.

[33] H. Qiu, L. Lv, B.-c. Pan, Q.-j. Zhang, W.-m. Zhang, and Q.-x. Zhang, "Critical review in adsorption kinetic models," *Journal of Zhejiang University-SCIENCE A*, vol. 10, no. 5, pp. 716–724, 2009, ISSN: 1862-1775. DOI: 10.1631/jzus.A0820524. [Online]. Available: https://link.springer.com/article/10.1631/jzus.A0820524.

[34] Y. S. Ho and G. McKay, "A comparison of chemisorption kinetic models applied to pollutant removal on various sorbents," *Process Safety and Environmental Protection*, vol. 76, no. 4, pp. 332–340, 1998, ISSN: 0957-5820. DOI: 10.1205/095758298529696. [Online]. Available: https://www.sciencedirect.com/science/article/pii/S0957582098707657.

[35] Y. S. Ho and G. McKay, "Sorption of dye from aqueous solution by peat," *Chemical Engineering Journal*, vol. 70, no. 2, pp. 115–124, 1998, ISSN: 1385-8947. DOI: 10.1016/S0923-0467(98)00076-1. [Online]. Available: https://www.sciencedirect.com/science/article/pii/S0923046798000761.

[36] N. S. Raghavan and D. M. Ruthven, "Numerical simulation of a fixed-bed adsorption column by the method of orthogonal collocation," *AIChE Journal*, vol. 29, no. 6, pp. 922–925, 1983, ISSN: 1547-5905. DOI: 10.1002/aic.690290608. [Online]. Available: https://aiche.onlinelibrary.wiley.com/doi/10.1002/aic.690290608.

[37] S. Whitaker, "Volume averaging of transport equations," in *Fluid transport in porous media*, ser. Advances in fluid mechanics, 1353-808X, J. P. Du Plessis, Ed., vol. 13, Southampton: Computational Mechanics, 1997, pp. 1–60, ISBN: 185312429X.

[38] H. Enwald, E. Peirano, and A.-E. Almstedt, "Eulerian two-phase flow theory applied to fluidization," *International Journal of Multiphase Flow*, vol. 22, pp. 21–66, 1996, ISSN: 0301-9322. DOI: 10.1016/S0301-9322(96)90004-X. [Online]. Available: https://www.sciencedirect.com/science/article/pii/S030193229690004X.

[39] S. Whitaker, *The Method of Volume Averaging* (Theory and Applications of Transport in Porous Media). Springer Netherlands, 2013, ISBN: 9789401733892.

[40] S. B. Höcker, R. Trunk, W. Dörfler, and M. J. Krause, "Towards the simulations of inertial dense particulate flows with a volume-averaged lattice boltzmann method," *Computers & Fluids*, vol. 166, pp. 152–162, 2018, ISSN: 00457930. DOI: 10.1016/j.compfluid.2018.02.011.

[41] B. D. Wood, F. Cherblanc, M. Quintard, and S. Whitaker, "Volume averaging for determining the effective dispersion tensor: Closure using periodic unit cells and comparison with ensemble averaging," *Water Resources Research*, vol. 39, no. 8, 2003, ISSN: 00431397. DOI: 10.1029/2002WR001723. [Online]. Available: https://agupubs.onlinelibrary.wiley.com/doi/full/10.1029/2002WR001723.

[42] M.-L. Maier, "Coupled lattice boltzmann and discrete element method for reactive particle fluid flows with applications in process engineering," Ph.D. dissertation, Karlsruhe Institut für Technologie, Karlsruhe, 2021.

[43] R. Trunk, T. Henn, W. Dörfler, H. Nirschl, and M. J. Krause, "Inertial dilute particulate fluid flow simulations with an euler–euler lattice boltzmann method," *Journal of Computational Science*, vol. 17, pp. 438–445, 2016, ISSN: 1877-7503. DOI: 10.1016/j.jocs.2016.03.013. [Online]. Available: https://www.sciencedirect.com/science/article/pii/S1877750316300345.

[44] P. R. Souza, G. L. Dotto, and N. Salau, "Detailed numerical solution of pore volume and surface diffusion model in adsorption systems," *Chemical Engineering Research and Design*, vol. 122, pp. 298–307, 2017, ISSN: 0263-8762. DOI: 10.1016/j.cherd.2017.04.021. [Online]. Available: https://www.sciencedirect.com/science/article/pii/S0263876217302514.

[45] W. R. Cowell, *Sources and development of mathematical software* (Prentice-Hall series in computational mathematics). Englewood Cliffs and London: Prentice-Hall, 1984, ISBN: 0138235015.

[46] D. Anderl, M. Bauer, C. Rauh, U. Rüde, and A. Delgado, "Numerical simulation of adsorption and bubble interaction in protein foams using a lattice boltzmann method," *Food & Function*, vol. 5, no. 4, pp. 755–763, 2014, ISSN: 2042-650X. DOI: 10.1039/C3FO60374A. [Online]. Available: https://pubs.rsc.org/en/content/articlelanding/2014/FO/c3fo60374a.

[47] T. Seta, "Implicit temperature-correction-based immersed-boundary thermal lattice boltzmann method for the simulation of natural convection," *Physical review. E, Statistical, nonlinear, and soft matter physics*, vol. 87, no. 6, p. 063 304, 2013. DOI: 10.1103/PhysRevE.87.063304.

[48] Z. Guo and T. S. Zhao, "Lattice boltzmann model for incompressible flows through porous media," *Physical review. E, Statistical, nonlinear, and soft matter physics*, vol. 66, no. 3 Pt 2B, p. 036 304, 2002. DOI: 10.1103/PhysRevE.66.036304. [Online]. Available: https://journals.aps.org/pre/pdf/10.1103/PhysRevE.66.036304 (visited on 02/05/2022).

[49] S. R. Lynch, N. Nama, Z. Xu, C. J. Arthurs, O. Sahni, and C. A. Figueroa, "Numerical considerations for advection-diffusion problems in cardiovascular hemodynamics," *International journal for numerical methods in biomedical engineering*, vol. 36, no. 9, e3378, 2020. DOI: 10.1002/cnm.3378. [Online]. Available: https://deepblue.lib.umich.edu/bitstream/handle/2027.42/162812/cnm3378.pdf?sequence=2 (visited on 05/20/2022).

[50] G. Gruszczyński, M. Dzikowski, and Ł. Łaniewski-Wołłk, *On recovering the second-order convergence of the lattice boltzmann method with reaction-type source terms*, 2021. [Online]. Available: https://arxiv.org/pdf/2107.03962.pdf (visited on 05/16/2022).

[51] M. Junk, A. Klar, and L.-S. Luo, "Asymptotic analysis of the lattice boltzmann equation," *Journal of Computational Physics*, vol. 210, no. 2, pp. 676–704, 2005, ISSN: 0021-9991. DOI: 10.1016/j.jcp.2005.05.003.

[52] J. H. Ferziger and M. Perić, *Computational Methods for Fluid Dynamics* (Springer eBook Collection), third, rev. edition. Heidelberg: Springer, 2002, ISBN: 9783642560262. DOI: 10.1007/978-3-642-56026-2.

[53] J. Crank, *The mathematics of diffusion* (Oxford science publications), 2nd ed. Oxford: Clarendon Press, 1975, ISBN: 0198533446. [Online]. Available: http://www-eng.lbl.gov/~shuman/NEXT/MATERIALS&COMPONENTS/Xe_damage/Crank-The-Mathematics-of-Diffusion.pdf (visited on 03/25/2022).

[54] C. Tien, *Adsorption calculations and modeling* (Butterworth-Heinemann series in chemical engineering). Boston and London: Butterworth-Heinemann, 1994, ISBN: 0-7506-9121-2.